Y.Azuma (Teijin Institute for Biomedical Research) for histomorphometric analysis, A.Asai and T.Kirino (Department of Neurosurgery, The University of Tokyo) for providing Bcl-xL adenovirus, H.Katagiri (Tohoku University) and T.Asano (The University of Tokyo) for MEK^{CA} and myrAKT adenoviruses, T.Kitamura (Institute of Medial Science, The University of Tokyo) for pMx vectors, and J.Adams and S.Cory (WEHI) for *bim−/−* mice. This work was supported by fellowships and Grants-in-Aid from the Ministry of Education, Science, Sports and Culture of Japan, the Health Science Research Grants from the Ministry of Health and Welfare of Japan, Uehara Memorial Award, Nakatomi Health Science Foundation Award, Grants-in-Aid from the Research Society for Metabolic Bone Diseases to S.T., and by the NHMRC (Canberra), the Leukemia and Lymphoma Society of America and the Dr Josef Steiner Cancer Research Foundation (Bern).

References

Akune,T. *et al.* (2002) Insulin receptor substrate-2 maintains predominance of anabolic function over catabolic function of osteoblasts. *J. Cell Biol.*, **159**, 147–156.

Baron,R. (1989) Molecular mechanisms of bone resorption by the osteoclast. *Anat. Rec.*, **224**, 317–324.

Biswas,S.C. and Greene,L.A. (2002) Nerve growth factor (NGF) down-regulates the Bcl-2 homology 3 (BH3) domain-only protein Bim and suppresses its proapoptotic activity by phosphorylation. *J. Biol. Chem.*, **277**, 49511–49516.

Bouillet,P., Metcalf,D., Huang,D.C., Tarlinton,D.M., Kay,T.W., Kontgen,F., Adams,J.M. and Strasser,A. (1999) Proapoptotic Bcl-2 relative Bim required for certain apoptotic responses, leukocyte homeostasis and to preclude autoimmunity. *Science*, **286**, 1735–1738.

Bouillet,P. *et al.* (2002) BH3-only Bcl-2 family member Bim is required for apoptosis of autoreactive thymocytes. *Nature*, **415**, 922–926.

Breitschopf,K., Zeiher,A.M. and Dimmeler,S. (2000) Ubiquitin-mediated degradation of the proapoptotic active form of bid. A functional consequence on apoptosis induction. *J. Biol. Chem.*, **275**, 21648–21652.

Cheng,E.H., Wei,M.C., Weiler,S., Flavell,R.A., Mak,T.W., Lindsten,T. and Korsmeyer,S.J. (2001) BCL-2, BCL-X(L) sequester BH3 domain-only molecules preventing BAX- and BAK-mediated mitochondrial apoptosis. *Mol. Cell*, **8**, 705–711.

Chiusaroli,R., Sanjay,A., Henriksen,K., Engsig,M.T., Horne,W.C., Gu,H. and Baron,R. (2003) Deletion of the gene encoding c-Cbl alters the ability of osteoclasts to migrate, delaying resorption and ossification of cartilage during the development of long bones. *Dev. Biol.*, **261**, 537–547.

Dijkers,P.F., Birkenkamp,K.U., Lam,E.W., Thomas,N.S., Lammers, J.W., Koenderman,L. and Coffer,P.J. (2002) FKHR-L1 can act as a critical effector of cell death induced by cytokine withdrawal: protein kinase B-enhanced cell survival through maintenance of mitochondrial integrity. *J. Cell Biol.*, **156**, 531–542.

Dimmeler,S., Breitschopf,K., Haendeler,J. and Zeiher,A.M. (1999) Dephosphorylation targets Bcl-2 for ubiquitin-dependent degradation: a link between the apoptosome and the proteasome pathway. *J. Exp. Med.*, **189**, 1815–1822.

Fuller,K., Owens,J.M., Jagger,C.J., Wilson,A., Moss,R. and Chambers,T.J. (1993) Macrophage colony-stimulating factor stimulates survival and chemotactic behavior in isolated osteoclasts. *J. Exp. Med.*, **178**, 1733–1744.

Glantschnig,H., Fisher,J.E., Wesolowski,G., Rodan,G.A. and Reszka,A.A. (2003) M-CSF, TNFα and RANK ligand promote osteoclast survival by signaling through mTOR/S6 kinase. *Cell Death Differ.*, **10**, 1165–1177.

Glickman,M.H. and Ciechanover,A. (2002) The ubiquitin–proteasome proteolytic pathway: destruction for the sake of construction. *Physiol. Rev.*, **82**, 373–428.

Gross,A., McDonnell,J.M. and Korsmeyer,S.J. (1999) BCL-2 family members and the mitochondria in apoptosis. *Genes Dev.*, **13**, 1899–1911.

Hattersley,G., Dorey,E., Horton,M.A. and Chambers,T.J. (1988) Human macrophage colony-stimulating factor inhibits bone resorption by osteoclasts disaggregated from rat bone. *J. Cell. Physiol.*, **137**, 199–203.

Haupt,Y., Maya,R., Kazaz,A. and Oren,M. (1997) Mdm2 promotes the rapid degradation of p53. *Nature*, **387**, 296–299.

Hentunen,T.A. *et al.* (1998) Immortalization of osteoclast precursors by targeting Bcl-XL and simian virus 40 large T antigen to the osteoclast lineage in transgenic mice. *J. Clin. Invest.*, **102**, 88–97.

Huang,D.C. and Strasser,A. (2000) BH3-only proteins—essential initiators of apoptotic cell death. *Cell*, **103**, 839–842.

Hughes,D.E., Wright,K.R., Uy,H.L., Sasaki,A., Yoneda,T., Roodman, G.D., Mundy,G.R. and Boyce,B.F. (1995) Bisphosphonates promote apoptosis in murine osteoclasts *in vitro* and *in vivo*. *J. Bone Miner. Res.*, **10**, 1478–1487.

Jesenberger,V. and Jentsch,S. (2002) Deadly encounter: ubiquitin meets apoptosis. *Nature Rev. Mol. Cell. Biol.*, **3**, 112–121.

Joazeiro,C.A. and Weissman,A.M. (2000) RING finger proteins: mediators of ubiquitin ligase activity. *Cell*, **102**, 549–552.

Kerr,J.F., Wyllie,A.H. and Currie,A.R. (1972) Apoptosis: a basic biological phenomenon with wide-ranging implications in tissue kinetics. *Br. J. Cancer*, **26**, 239–257.

Kobayashi,N., Kadono,Y., Naito,A., Matsumoto,K., Yamamoto,T., Tanaka,S. and Inoue,J. (2001) Segregation of TRAF6-mediated signaling pathways clarifies its role in osteoclastogenesis. *EMBO J.*, **20**, 1271–1280.

Kubbutat,M.H., Jones,S.N. and Vousden,K.H. (1997) Regulation of p53 stability by Mdm2. *Nature*, **387**, 299–303.

Lee,K., Deeds,J.D. and Segre,G.V. (1995) Expression of parathyroid hormone-related peptide and its receptor messenger ribonucleic acids during fetal development of rats. *Endocrinology*, **136**, 453–463.

Lei,K. and Davis,R.J. (2003) JNK phosphorylation of Bim-related members of the Bcl2 family induces Bax-dependent apoptosis. *Proc. Natl Acad. Sci. USA*, **100**, 2432–2437.

Ley,R., Balmanno,K., Hadfield,K., Weston,C.R. and Cook,S.J. (2003) Activation of the ERK1/2 signalling pathway promotes phosphorylation and proteasome-dependent degradation of the BH3-only protein Bim. *J. Biol. Chem.*, **278**, 18811–18816.

Marshansky,V., Wang,X., Bertrand,R., Luo,H., Duguid,W., Chinnadurai,G., Kanaan,N., Vu,M.D. and Wu,J. (2001) Proteasomes modulate balance among proapoptotic and antiapoptotic Bcl-2 family members and compromise functioning of the electron transport chain in leukemic cells. *J. Immunol.*, **166**, 3130–3142.

Miyazaki,T. *et al.* (2000) Reciprocal role of ERK and NF-κB pathways in survival and activation of osteoclasts. *J. Cell Biol.*, **148**, 333–342.

Miyazaki,T., Neff,L., Tanaka,S., Horne,W.C. and Baron,R. (2003) Regulation of cytochrome c oxidase activity by c-Src in osteoclasts. *J. Cell Biol.*, **160**, 709–718.

Mochizuki,T. *et al.* (2002) Akt protein kinase inhibits non-apoptotic programmed cell death induced by ceramide. *J. Biol. Chem.*, **277**, 2790–2797.

Naramura,M., Kole,H.K., Hu,R.J. and Gu,H. (1998) Altered thymic positive selection and intracellular signals in Cbl-deficient mice. *Proc. Natl Acad. Sci. USA*, **95**, 15547–15552.

O'Connor,L., Strasser,A., O'Reilly,L.A., Hausmann,G., Adams,J.M., Cory,S. and Huang,D.C. (1998) Bim: a novel member of the Bcl-2 family that promotes apoptosis. *EMBO J.*, **17**, 384–395.

Okahashi,N., Koide,M., Jimi,E., Suda,T. and Nishihara,T. (1998) Caspases (interleukin-1β-converting enzyme family proteases) are involved in the regulation of the survival of osteoclasts. *Bone*, **23**, 33–41.

O'Reilly,L.A., Cullen,L., Visvader,J., Lindeman,G.J., Print,C., Bath, M.L., Huang,D.C. and Strasser,A. (2000) The proapoptotic BH3-only protein bim is expressed in hematopoietic, epithelial, neuronal and germ cells. *Am. J. Pathol.*, **157**, 449–461.

Putcha,G.V., Moulder,K.L., Golden,J.P., Bouillet,P., Adams,J.A., Strasser,A. and Johnson,E.M. (2001) Induction of BIM, a proapoptotic BH3-only BCL-2 family member, is critical for neuronal apoptosis. *Neuron*, **29**, 615–628.

Sanjay,A. *et al.* (2001) Cbl associates with Pyk2 and Src to regulate Src kinase activity, α(v)β(3) integrin-mediated signaling, cell adhesion and osteoclast motility. *J. Cell Biol.*, **152**, 181–195.

Shinjyo,T. *et al.* (2001) Downregulation of Bim, a proapoptotic relative of Bcl-2, is a pivotal step in cytokine-initiated survival signaling in murine hematopoietic progenitors. *Mol. Cell. Biol.*, **21**, 854–864.

Strasser,A., Harris,A.W., Huang,D.C., Krammer,P.H. and Cory,S. (1995) Bcl-2 and Fas/APO-1 regulate distinct pathways to lymphocyte apoptosis. *EMBO J.*, **14**, 6136–6147.

Strasser,A., O'Connor,L. and Dixit,V.M. (2000) Apoptosis signaling. *Annu. Rev. Biochem.*, **69**, 217–245.

Suda,T., Takahashi,N. and Martin,T.J. (1992) Modulation of osteoclast differentiation. *Endocr. Rev.*, **13**, 66–80.

Taher,T.E., Tjin,E.P., Beuling,E.A., Borst,J., Spaargaren,M. and Pals,S.T. (2002) c-Cbl is involved in Met signaling in B cells and

mediates hepatocyte growth factor-induced receptor ubiquitination. *J. Immunol.*, **169**, 3793–3800.

Takahashi,N., Akatsu,T., Udagawa,N., Sasaki,T., Yamaguchi,A., Moseley,J.M., Martin,T.J. and Suda,T. (1988) Osteoblastic cells are involved in osteoclast formation. *Endocrinology*, **123**, 2600–2602.

Tanaka,S., Amling,M., Neff,L., Peyman,A., Uhlmann,E., Levy,J.B. and Baron,R. (1996) c-Cbl is downstream of c-Src in a signalling pathway necessary for bone resorption. *Nature*, **383**, 528–531.

Tanaka,S., Takahashi,T., Takayanagi,H., Miyazaki,T., Oda,H., Nakamura,K., Hirai,H. and Kurokawa,T. (1998) Modulation of osteoclast function by adenovirus vector-induced epidermal growth factor receptor. *J. Bone Miner. Res.*, **13**, 1714–1720.

Tanaka,S., Nakamura,I., Inoue,J., Oda,H. and Nakamura,K. (2003) Signal transduction pathways regulating osteoclast differentiation and function. *J. Bone Miner. Metab.*, **21**, 123–133.

Thompson,C.B. (1995) Apoptosis in the pathogenesis and treatment of disease. *Science*, **267**, 1456–1462.

Villunger,A., Scott,C., Bouillet,P. and Strasser,A. (2003) Essential role for the BH3-only protein Bim but redundant roles for Bax, Bcl-2 and Bcl-w in the control of granulocyte survival. *Blood*, **101**, 2393–2400.

Weston,C.R., Balmanno,K., Chalmers,C., Hadfield,K., Molton,S.A., Ley,R., Wagner,E.F. and Cook,S.J. (2003) Activation of ERK1/2 by ΔRaf-1: ER* represses Bim expression independently of the JNK or PI3K pathways. *Oncogene*, **22**, 1281–1293.

Whitfield,J., Neame,S.J., Paquet,L., Bernard,O. and Ham,J. (2001) Dominant-negative c-Jun promotes neuronal survival by reducing BIM expression and inhibiting mitochondrial cytochrome c release. *Neuron*, **29**, 629–643.

Wong,B.R., Besser,D., Kim,N., Arron,J.R., Vologodskaia,M., Hanafusa,H. and Choi,Y. (1999) TRANCE, a TNF family member, activates Akt/PKB through a signaling complex involving TRAF6 and c-Src. *Mol. Cell*, **4**, 1041–1049.

Yamaguchi,T., Okada,T., Takeuchi,K., Tonda,T., Ohtaki,M., Shinoda,S., Masuzawa,T., Ozawa,K. and Inaba,T. (2003) Enhancement of thymidine kinase-mediated killing of malignant glioma by BimS, a BH3-only cell death activator. *Gene Ther.*, **10**, 375–385.

Yang,Y., Fang,S., Jensen,J.P., Weissman,A.M. and Ashwell,J.D. (2000) Ubiquitin protein ligase activity of IAPs and their degradation in proteasomes in response to apoptotic stimuli. *Science*, **288**, 874–877.

Zong,W.X., Lindsten,T., Ross,A.J., MacGregor,G.R. and Thompson, C.B. (2001) BH3-only proteins that bind pro-survival Bcl-2 family members fail to induce apoptosis in the absence of Bax and Bak. *Genes Dev.*, **15**, 1481–1486.

Received July 10, 2003; revised October 27, 2003; accepted October 30, 2003

JOURNAL OF CELLULAR PHYSIOLOGY 197:348–356 (2003)

Contribution of Membrane-Associated Prostaglandin E_2 Synthase to Bone Resorption

MASATOMO SAEGUSA,[1,2] MAKOTO MURAKAMI,[2] YOSHIHITO NAKATANI,[2] KIYOFUMI YAMAKAWA,[1] MIKA KATAGIRI,[1] KOICHI MATSUDA,[1] KOZO NAKAMURA,[1] ICHIRO KUDO,[2] AND HIROSHI KAWAGUCHI[1]*

[1]*Department of Orthopaedic Surgery, Faculty of Medicine, University of Tokyo, Tokyo, Japan*

[2]*Department of Health Chemistry, School of Pharmaceutical Sciences, Showa University, Tokyo, Japan*

This study initially confirmed that, among prostaglandins (PGs) produced in bone, only PGE_2 has the potency to stimulate osteoclastogenesis and bone resorption in the mouse coculture system of osteoblasts and bone marrow cells. For the PGE_2 biosynthesis two isoforms of the terminal and specific enzymes, membrane-associated PGE_2 synthase (mPGES) and cytosolic PGES (cPGES) have recently been identified. In cultured mouse primary osteoblasts, both mPGES and cyclooxygenase-2 were induced by the bone resorptive cytokines interleukin-1, tumor necrosis factor-α, and fibroblast growth factor-2. Induction of mPGES was also seen in the mouse long bone and bone marrow in vivo by intraperitoneal injection of lipopolysaccharide. In contrast, cPGES was expressed constitutively both in vitro and in vivo without being affected by these stimuli. An antisense oligonucleotide blocking mPGES expression inhibited not only PGE_2 production, but also osteoclastogenesis and bone resorption stimulated by the cytokines, which was reversed by addition of exogenous PGE_2. We therefore conclude that mPGES, which is induced by and mediates the effects of bone resorptive stimuli, may make a target molecule for the treatment of bone resorptive disorders. J. Cell. Physiol. 197: 348–356, 2003. © 2003 Wiley-Liss, Inc.

Prostanoids are important mediators that play a variety of roles in biological events, such as fever, pain, inflammation, tumorigenesis, gastrointestinal protection, vascular circulation, and bone metabolism (Raisz, 1995; Kawaguchi et al., 1995a; Funk, 2001; Harris et al., 2002). Prostaglandin E_2 (PGE_2), $PGF_{2\alpha}$, PGI_2, and thromboxane B_2 are accumulated in bone and are produced by cells of the osteoblast lineage (Raisz, 1995; Kawaguchi et al., 1995a). These PGs are multifunctional regulators with both stimulatory and inhibitory effects on bone formation and resorption. However, the major effect of PGs has been recognized as the stimulation of bone resorption since PGE_2 was first shown to increase cyclic AMP and stimulate resorption in cultured fetal rat long bones more than 30 years ago (Klein and Raisz, 1970). Many factors including cytokines and systemic hormones, which are involved in regulation of bone resorption, also regulate PG production in bone (Kawaguchi et al., 1994, 1995a,b; Raisz, 1995). In addition, resorptive responses to cytokines and hormones are often, at least in part, dependent on PG production since nonsteroidal anti-inflammatory drugs (NSAIDs) inhibit these responses (Akatsu et al., 1989, 1991; Shinar and Rodan, 1990; Kawaguchi et al., 2000). In vivo studies in animals and humans also suggest that PGs could be responsible for bone resorptive disorders, such as postmenopausal bone loss (Kawaguchi et al., 1995c), hypercalcemia of malignancy (Tashjian et al., 1977; Minkin et al., 1981), inflammatory bone loss in periodontal disease (Harris et al., 1973; Harvey et al.,

Abbreviations: PG, prostaglandin; mPGES, membrane-associated prostaglandin E_2 synthase; cPGES, cytosolic prostaglandin E_2 synthase; COX, cyclooxygenase; IL, interleukin; TNF, tumor necrosis factor; FGF, fibroblast growth factor; NSAIDs, nonsteroidal anti-inflammatory drugs; LPS, lipopolysaccharide; MGST1-L1, microsomal glutathione S-transferase 1-like 1; RA, rheumatoid arthritis; αMEM, alpha modified-minimum essential medium; FBS, fetal bovine serum; PBS, phosphate buffered saline; TRAP, Tartrate resistant acid phosphatase; SDS, sodium dodecyl sulfate; RANKL, receptor activator of nuclear factor-κB ligand; RT-PCR, reverse transcriptase-polymerase chain reaction; PVDF, polyvinyl difluoride; ELISA, enzyme-linked immunosorbent assay; ECL, enhanced chemiluminescence.

Contract grant sponsor: Japanese Ministry of Education, Science, Sports and Culture; Contract grant number: 14370452; Contract grant sponsor: Nakatomi Health & Science Grant.

*Correspondence to: Hiroshi Kawaguchi, Department of Orthopaedic Surgery, Faculty of Medicine, University of Tokyo, Hongo 7-3-1, Bunkyo-ku, Tokyo 113-8655, Japan.
E-mail: kawaguchi-ort@h.u-tokyo.ac.jp

Received 19 February 2003; Accepted 5 May 2003

DOI: 10.1002/jcp.10356

1984), loosening of joint replacements (Goldring et al., 1983; Horowitz et al., 1994), and joint destruction in rheumatoid arthritis (RA) (Robinson et al., 1975; Manabe et al., 1999).

PGE_2 is the most abundant prostanoid among PGs in bone and has been believed to be the most potent bone resorber (Raisz, 1995; Kawaguchi et al., 1995a). PGE_2 exerts its resorptive action by inducing receptor activator of nuclear factor κB ligand (RANKL) on osteoblastic cells through an autocrine/paracrine mechanism, which elicits the support of osteoclast differentiation from hemopoietic precursors (Suda et al., 1999). PGI_2 is the next most abundant PG in bone (Raisz, 1995; Kawaguchi et al., 1995a), but it does not appear to be an important mediator of the bone resorptive response (Tashjian et al., 1988). Small amounts of $PGF_{2\alpha}$ are produced by bone cells and exogenous $PGF_{2\alpha}$ can stimulate bone resorption; however, its effect appears to be due to an increase in endogenous PGE_2 production (Raisz et al., 1990). In the present study we initially performed a comprehensive and comparative examination among prostanoids accumulated in bone on their potency to resorb bone using two mouse assay systems, and confirmed that only PGE_2 can stimulate osteoclastogenesis and bone resorption.

PGE_2 production from arachidonic acid, which is released by phospholipase A_2 from membrane phospholipids, is regulated by two rate-limiting steps. The first step is catalyzed by cyclooxygenase (COX), which converts arachidonic acid to the intermediate prostanoid PGH_2. Two isoforms of the COX enzyme have been identified: COX-1, which is a constitutive enzyme; and COX-2, which is induced by various stimuli, including cytokines, hormones, and lipopolysaccharide (LPS) (Smith and Langenbach, 2001). The second step is the terminal conversion reaction of PGH_2 to PGE_2, which is catalyzed by PGE_2 synthase (PGES). At least two forms of the PGES enzyme have recently been identified (Jakobsson et al., 1999; Tanioka et al., 2000). Cytosolic PGES (cPGES), which is identical to the heat shock protein 90-associated protein p23, is expressed ubiquitously and unaltered by proinflammatory stimuli in a wide variety of cells and tissues and promotes COX-1-mediated immediate PGE_2 production (Tanioka et al., 2000). This COX-1 and cPGES coupling is assumed to contribute to the production of PGE_2, which plays a role in the maintenance of tissue homeostasis. Contrarily, membrane-associated PGES (mPGES), which was originally designated microsomal glutathione S-transferase 1-like 1 (MGST1-L1), is an inducible enzyme, which is coordinately induced with COX-2 on the perinuclear membrane and is functionally coupled with COX-2 in marked preference to COX-1 (Jakobsson et al., 1999; Murakami et al., 2000). mPGES expression is induced by proinflammatory stimuli in various tissues and cells and was down-regulated by dexamethasone, accompanied by changes in COX-2 expression and subsequent PGE_2 production (Jakobsson et al., 1999; Murakami et al., 2000). COX-2 and mPGES are therefore thought to be essential components for PGE_2 biosynthesis, which may be linked to several pathological conditions such as inflammation, fever and cancer (Satoh et al., 2000; Filion et al., 2001; Mancini et al., 2001).

We have reported that COX-2 is abundantly expressed in osteoblasts and plays a central role in the biosynthesis of PGE_2 in response to several stimuli of bone resorption (Pilbeam et al., 1993; Kawaguchi et al., 1994, 1995b, 1996, 2000; Chikazu et al., 2001). A previous mouse co-culture experiment revealed that osteoclast formation was significantly reduced in cultures of cells derived from mice lacking COX-2 relative to wild-type cultures, an effect that could be reversed by providing exogenous PGE_2 (Okada et al., 2000a). We also demonstrated the involvement of COX-2 induction and subsequent PGE_2 production by cytokines: interleukin-1 (IL-1), tumor necrosis factor-α (TNF-α), and fibroblast growth factor-2 (FGF-2), in the bone resorptive disorders postmenopausal osteoporosis and RA joint destruction (Kawaguchi et al., 1995c; Manabe et al., 1999). In this study we examined the expression of mPGES and its regulation by these bone resorptive cytokines in bone in vitro and in vivo. To further investigate the possibility of mPGES as a novel target for the development of drugs that are highly selective for bone resorptive diseases with low side effects on other tissue homeostasis, we examined the contribution of endogenous mPGES to bone resorption using an antisense oligonucleotide against mPGES.

MATERIALS AND METHODS

Materials

Neonatal and 8-week-old ddY mice were purchased from Shizuoka Laboratories Animal Center (Shizuoka, Japan). Human recombinant FGF-2 was provided by Kaken Pharmaceutical Co., Ltd. (Chiba, Japan). Mouse TNF-α was purchased from Genzyme (Cambridge, MA). Rabbit anti-mouse mPGES, COX-1, COX-2 antibodies were purchased from Cayman Chemical (Ann Arbor, MI). A rabbit anti-human cPGES antiboby, which has been confirmed to cross-react with mouse cPGES, was prepared by the immunization of rabbits as previously reported (Tanioka et al., 2000). Anti-rabbit IGG HRP Conjugate was purchased from Promega (Madison, WI). The reverse transcriptase-polymerase chain reaction (RT-PCR) kit was from Takara Biomedicals (Shiga, Japan). Bacterial collagenase and $1,25(OH)_2$ vitamin D_3 were purchased from Wako Pure Chemicals Co. (Osaka, Japan), and dispase from Nitta Gelatin Co. (Osaka, Japan). LPS and NS-398 were purchased from Calbiochem (San Diego, CA). Alpha modified-minimum essential medium (αMEM) was purchased from GIBCO BRL (Rockville, MD), and fetal bovine serum (FBS) was from the Cell Culture Laboratory (Cleveland, OH). Other chemicals were obtained from Sigma Chemical Company (St. Louis, MO).

Mouse primary osteoblast culture

All animal experiments were performed according to the guidelines of the International Association for the Study of Pain (Zimmermann, 1983). In addition, the experimental work was reviewed by the committee of Tokyo University, charged with confirming ethics. Calvariae dissected from 1- to 4-day-old mice were washed in phosphate buffered saline (PBS) and digested with 1 ml of trypsin/EDTA (GIBCO BRL) containing 10 mg collagenase (Sigma, type 7) for 10 min five times, and cells from fractions 3 to 5 were pooled. Cells were

plated in 6-multiwell dishes at a density of 5,000 cells/cm^2 and grown to confluence in αMEM containing 10% FBS, penicillin (50 U/ml), streptomycin (50 mg/ml), and 0.2 mM L-ascorbic acid phosphate ester sodium salt in a humidified CO_2 incubator.

Tartrate resistant acid phosphatase (TRAP)-positive multinucleated osteoclast formation in the coculture of mouse primary osteoblasts and bone marrow cells

Mouse calvarial primary osteoblasts described above (2×10^4 cells/well) and bone marrow cells prepared from 8-week-old mice (1×10^6 cells/well) were cocultured in 24-multiwell dishes containing αMEM/10% FBS with and without prostanoids, 1,25$(OH)_2$ vitamin D_3, IL-1α, and oligonucleotides as described below for 6 days with a medium change at 3 days. After 6 days of culture, the cells were fixed with 3.7% formaldehyde in PBS and ethanol-acetone (50:50, vol/vol), and stained at pH 5.0 in the presence of L(+)-tartaric acid using naphtol AS-MX phosphate in N,N-dimethyl formamide as the substrate. The number of TRAP-positive-multinucleated cells containing more than three nuclei was counted as osteoclasts.

Resorbed pit formation assay in the coculture of mouse primary osteoblasts and bone marrow cells

Mouse osteoblasts (1×10^6 cells/dish) and bone marrow cells (5×10^7 cells/dish) prepared as above were cocultured on 10-cm culture dishes coated with 0.24% collagen gel matrix (Nitta Gelatin, Tokyo, Japan) containing αMEM/10% FBS with and without prostanoids, 1,25$(OH)_2$ vitamin D_3, IL-1α, and oligonucleotides as described below for 6 days with a medium change every 3 days. Non adherent cells were then washed with PBS and adherent cells were stripped by 0.2% bacterial collagenase. An aliquot of the crude cell preparation (0.1 ml) was further cultured on a dentine slice placed in each well of 96-well dishes containing αMEM/10% FBS with and without the same agents as the previous culture. After 24 h of culture, cells were removed with 1 N NH_4OH solution, and stained with 0.5% toluidine blue. Total area was estimated under a light microscope with a micrometer to assess osteoclastic bone resorption using an image analyzer (System Supply Co., Nagano, Japan).

Northern blot analysis

Mouse primary osteoblasts were cultured as described above, changed to the same medium 24 h before cytokines stimulations {IL-1α (10 ng/ml), TNF-α (10 ng/ml), and FGF-2 (10 nM)} and cultured for the indicated periods. Total RNA was extracted using ISOGEN (Wako Pure Chemicals Co.) according to the manufacturer's instructions. Equal amounts (10–20 μg) were electrophoresed in 1.2% agarose-formaldehyde gel and transferred onto nylon membrane filters (Hybond-N; Amersham International, Little Chalfont, UK). The resulting blots were then probed with the respective cDNA probes shown in previous reports (Murakami et al., 2000; Tanioka et al., 2000) that had been labeled with [^{32}P]dCTP (Amersham Pharmacia Biotech, Inc., Tokyo, Japan) by random priming (Takara Biomedicals) according to the manufacturer's protocol. After washing, the filter was exposed to films at −80°C for 24 h to 1 week.

Western blot analysis

Mouse primary osteoblasts were cultured for indicated periods as described above, and were then collected by trypsin/EDTA and lysed in PBS containing 0.1% sodium dodecyl sulfate (SDS) to the final concentraion of 1×10^7 cells/ml. Equivalent amounts of cell lysates (10 μl containing 1×10^5 cells) were electrophoresed on the 4–20% gradient gel (Tris-Glysine Gel, Invitrogen, Carlsbad, CA), and transferred onto PVDF membrane (BIO-RAD, Hercules, CA). After blocking with 10 mM Tris-HCl containing 150 mM NaCl, 0.1% Tween 20 (TBS-T), and 5% skim milk, the membrane was incubated with antibodies against mPGES, cPGES, COX-2, and actin in TBS-T overnight at 4°C, and further with an anti-rabbit IgG horseradish peroxidase conjugate for 2 h. Reactive proteins were visualized using the enhanced chemiluminescence (ECL; Amersham Co., Arlington Heights, IL) following the manufacturer's instructions.

Intraperitoneal LPS injection

Eight-week-old ddY mice were intraperitoneally injected with 0.5 or 5.0 mg/kg of bacterial endotoxin LPS, which is known to evoke an acute inflammatory response (Fry et al., 1980). Control mice were injected with equivalent amounts of the vehicle PBS. After 3 and 6 h, animals were sacrificed and the whole femora and tibiae were excised. To extract RNA from the bone marrow and the residual bone from which bone marrow was removed, epiphyses at both ends were cut off, bone marrow was flushed with PBS, collected cells were suspended in ISOGEN extraction buffer, and total RNA was extracted. The residual bones were washed with PBS and immediately put into ISOGEN extraction buffer.

Semiquantitative RT-PCR and Southern blotting

Semiquantitative RT-PCR was performed within an exponential phase of the amplification. Total mRNA (1 μg) was reverse transcribed using Super Script reverse transcriptase with random hexamer (Takara Biomedicals), and 5% of the reaction mixture was amplified with LA-Taq DNA polymerase (Takara Biomedicals) using specific primer pairs: 5′-ATGCCTTCCCCGGGCCTGGTG-3′ and 5′-TGGTCACAGATGGTGGGCCAC-3′ for mPGES; 5′-AGGAAGCGATAATTTTAAGC-3′ and 5′-ACCCATGTGATCCATCATCTC-3′ for cPGES; 5′-GCATCGCTCTGTTCCTGTA-3′ and 5′-GTGCTCCCTCCTTTCATCA-3′ for RANKL; 5′-TGAAGGTCGGTGTGAACGGATTTGGC-3′ and 5′-CATGTAGGCCATGAGGTCCACCAC-3′ for G3PDH. The cycling parameters were 5 sec at 94°C and 4 min at 65°C for 25 cycles for mPGES; 45 sec at 94°C, 1 min at 49°C and 1 min at 72°C for 28 cycles for cPGES; 30 sec at 94°C, 30 sec at 56°C and 1.5 min at 72°C for 20 cycles for RANKL and G3PDH. Following PCR amplification, samples were electrophoresed on 1.0% agarose gels and transferred to nylon membrane filters. For the Southern blotting, the resulting blots were then probed with the mPGES cDNA probe above that had been labeled with [^{32}P]dCTP (Amersham Pharmacia Biotech) by random

priming (Takara Biomedicals) according to the manufacturer's instruction.

Antisense oligonucleotide

To examine the role of endogenous mPGES, its antisense oligonucleotide was synthesized. This was designed on the basis of the sequence of targeted to first ATG in mPGES: 5′-GGCCCGGGGAAGGCAT-3′. A random sequence oligonucleotide was used as a control: 5′-CCTCTTACCTCAGTTA-3′. To protect the oligonucleotide from degradation, a phosphorothioate oligonucleotide was synthesized commercially by Amersham Pharmacia Biotech. These oligonucleotides at the final concentration of 1 μg/ml were added to cultured primary osteoblasts and then cocultured with bone marrow cells for 4 h before IL-1α (10 ng/ml) or PGE_2 (10^{-6} M) treatment. RANKL mRNA level and PGE_2 in the supernatants of were measured by semiquantitative RT-PCR and enzyme-linked immunosorbent assay (ELISA) (Cayman Chemical), respectively, at 12 h after the stimulation in the osteoblast culture. The number of TRAP-positive multinucleated osteoclasts and the resorbed pit formation on a dentine slice were evaluated as described above.

Statistical analysis

Means of groups were compared by ANOVA and significance of differences was determined by post-hoc testing using Bonferroni's method.

RESULTS

Osteoclastogenesis and bone resorption by prostanoids in bone

Among prostanoids, PGE_2, $PGF_{2\alpha}$, PGI_2, and thromboxane B_2 are known to be produced and accumulated in bone (Raisz, 1995; Kawaguchi et al., 1995a). To begin with, we performed a comprehensive and comparative study to investigate, which of these prostanoids can affect osteoclastogenesis and bone resorption by measuring the number of TRAP-positive multinucleated osteoclasts (Fig. 1A) and the area of resorption pit on a dentine slice (Fig. 1B), respectively, in the coculture system of mouse primary osteoblasts and bone marrow cells. PGE_2 dose-dependently stimulated osteoclastogenesis up to a level similar to that of $1,25(OH)_2D_3$, although other prostanoids hardly affected them (Fig. 1A). When osteoclasts formed in the coculture were transferred onto the dentine slice and further cultured with and without these prostanoids, only PGE_2 showed the potency to stimulate resorbed pit formation. $PGF_{2\alpha}$ showed slight stimulation of osteoclastogenesis and pit formation as reported previously (Raisz et al., 1990), although the effects were not significant. These results suggest that among prostanoids in bone only PGE_2 has the potency to stimulate osteoclastic bone resorption. Hence, to elucidate the regulation of bone resorption through PGE_2, we further investigated the regulation and function of the terminal and specific enzyme PGES in bone.

Induction of mPGES in cultured osteoblasts by bone resorptive cytokines

We first examined the regulation of expressions of mPGES and cPGES by bone resorptive cytokines, IL-1α, TNF-α, and FGF-2, in cultured mouse primary osteoblasts. Figure 2A shows the time course of effects of the bone resorptive cytokines on the mRNA levels determined by Northern blotting in primary osteoblasts. mPGES induction by IL-1α and TNF-α was observed at 1–2 h, peaked around 3 h, and decreased thereafter, while that by FGF-2 was detected at 3–6 h and increased up to 48 h. This time course of mPGES transcript induction was similar to that of COX-2. Western blot analysis confirmed induction of the mPGES protein level by these cytokines (Fig. 2B). It was stimulated by bone resorptive cytokines at 6–12 h and maintained or increased thereafter up to 48 h, while the COX-2 protein level was stimulated earlier at 3 h and decreased after 12 h. In contrast to the induction of mPGES, both mRNA and protein level of cPGES was expressed constitutively without being much affected by these cytokines (Fig. 2A,B).

Induction of mPGES in bone marrow and the residual bone by intraperitoneal injection of LPS

To investigate PGES expression in vivo, an intraperitoneal injection of LPS (0.5 and 5 mg/kg) or PBS was administered to mice. After 3 and 6 h of injection, tibiae and femora were extracted, and the bone marrow and the residual bone were separated. mPGES mRNA level determined by RT-PCR/Southern blotting was upregulated by LPS injection dose-dependently in both bone marrow and the residual bone (Fig. 3). The induction seemed transient because it was stronger at 3 h than at 6 h in both tissues. cPGES mRNA level determined by RT-PCR was not affected by LPS injection in either tissue.

Contribution of mPGES to osteoclastic bone resorption

To examine the contribution of mPGES to bone resorption, we synthesized a phosphorothioate antisense oligonucleotide against mPGES. The antisense oligonucleotide was confirmed by Western blot analysis to inhibit the protein level of mPGES, but not that of COX-2, in the primary osteoblast culture with and without IL-1α stimulation (Fig. 4A). It also reduced medium PGE_2 and RANKL mRNA levels in the same cultures as compared to the control oligonucleotide (Fig. 4B). To learn the effect of this antisense oligonucleotide on osteoclastic bone resorption, it was added to cultured primary osteoblasts, which were then cocultured with bone marrow cells with and without IL-1α or PGE_2. In the control and IL-1α-stimulated cultures, the antisense oligonucleotide significantly reduced both osteoclastogenesis and resorbed pit formation on the dentine slice, while the control oligonucleotide changed neither of them (Fig. 4C). These inhibitions by the mPGES antisense oligonucleotide were similarly seen in the cocultures stimulated by TNF-α and FGF-2 (data not shown). NS-398, a specific COX-2 inhibitor, also decreased osteoclastogenesis and resorbed pit formation to levels similar to those of the mPGES antisense oligonucleotide. Neither the mPGES antisense oligonucleotide nor NS-398, however, could inhibit the osteoclastogenesis and resorbed pit formation stimulated by exogenous PGE_2. These results demonstrate that mPGES as well as COX-2 is an essential mediator of

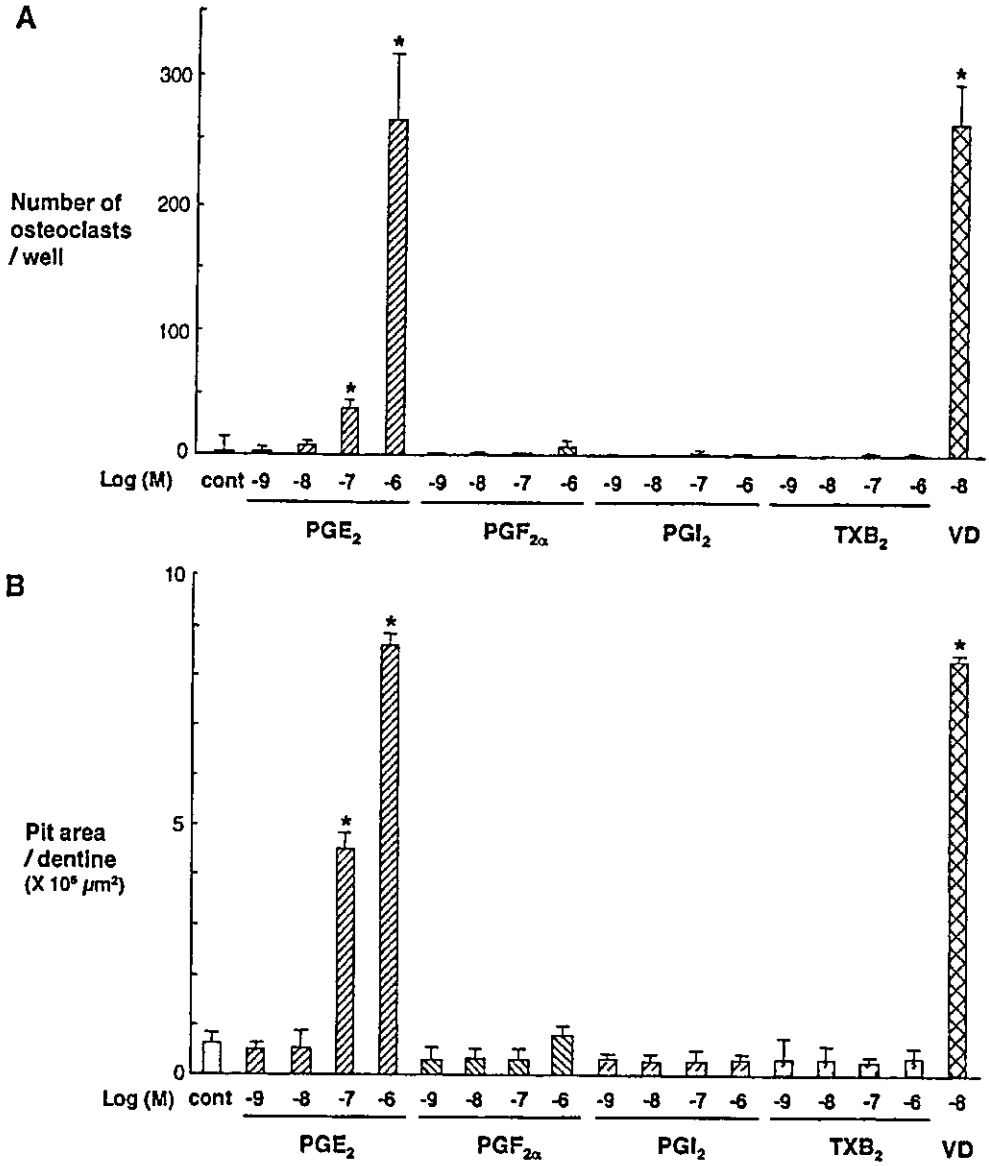

Fig. 1. Osteoclastogenesis (A) and bone resorption (B) by prostanoids in bone. A: Effect of prostanoids on osteoclastogenesis determined by the number of TRAP-positive multinucleated osteoclasts in the coculture system of mouse primary osteoblasts and bone marrow cells. These cells were cocultured with and without various concentrations (10^{-9}–10^{-6} M) of prostanoids (PGE_2, $PGF_{2\alpha}$, PGI_2, and TXB_2) or a positive control $1,25(OH)_2$ vitamin D_3 (10^{-8} M) for 6 days. The number of TRAP-positive cells containing more than three nuclei was counted as osteoclasts. B: Effect of prostanoids on bone resorption determined by the area of resorption pit on a dentine slice by the crude fraction of osteoclasts formed in the coculture above. An aliquot of the cell preparation formed in the coculture on collagen gel matrix was stripped and further cultured on a dentine slice for 24 h with the same agent as the previous coculture. *$P < 0.01$, significant difference from the control culture. Data are expressed as means (bars) ± SEMs (error bars) for eight cultures/group.

bone resorption by several cytokines through the production of PGE_2.

DISCUSSION

Based on the fact that PGE_2 was the only prostanoid that had the potency to stimulate osteoclastic bone resorption, in this study we examined the expression and the function of the terminal and specific enzyme of PGE_2 biosynthesis, PGES, in bone. Since mPGES was shown to be induced by and to mediate effects of bone resorptive stimuli, this enzyme may play an important role in physiological and pathological bone resorption.

Accumulated evidence has shown that mPGES is an inducible enzyme, the expression of which is markedly increased just like COX-2 in various cells and tissues following several stimuli (Jakobsson et al., 1999; Murakami et al., 2000; Soler et al., 2000; Stichtenoth et al., 2001; Yamagata et al., 2001; Han et al., 2002). Inducible genes usually contain particular nucleotide

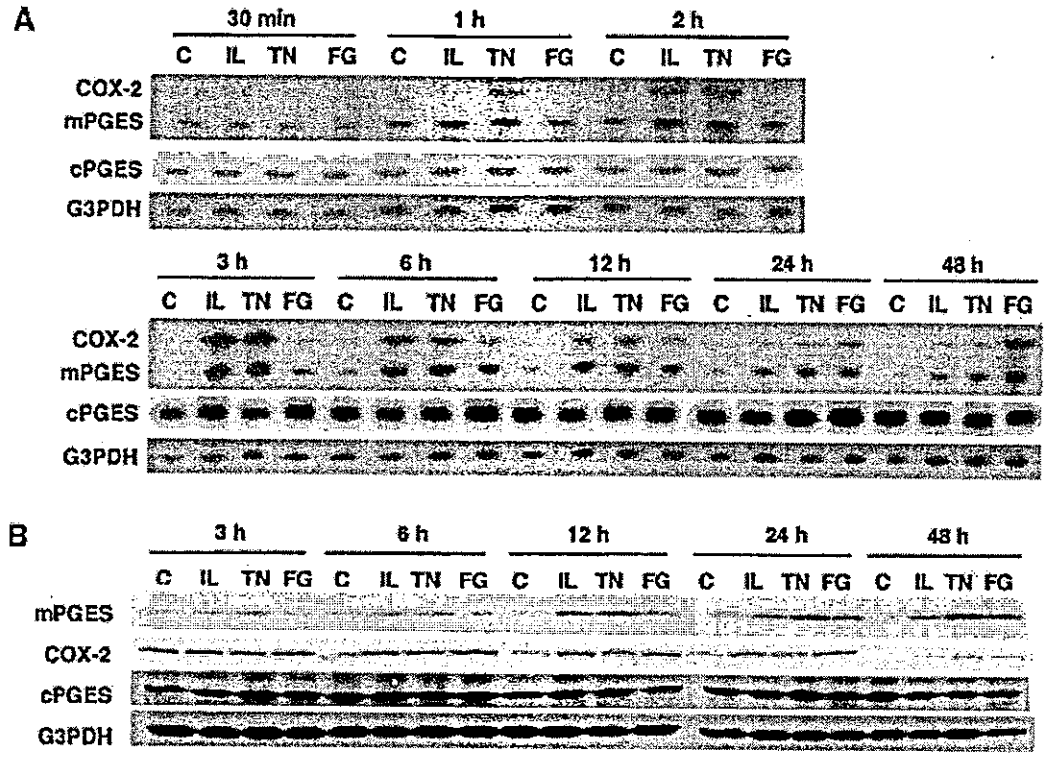

Fig. 2. Time course of effects of bone resorptive cytokines on mPGES, cPGES and COX-2 expressions in cultured mouse primary osteoblasts. A: mRNA levels of these enzymes in the control culture (C) and the IL-1α (IL, 10 ng/ml), TNF-α (TN, 10 ng/ml) or FGF-2 (FG, 10 nM)-stimulated cultures of primary osteoblasts for the indicated periods (30 min to 48 h) determined by Northern blot analysis. B: Protein levels of these enzymes in the control and stimulated cultures of primary osteoblasts for the indicated periods (3–48 h) determined by Western blot analysis.

elements within their promoter regions that are responsible for regulated transcription. In fact, a number of studies have reported the transcriptional regulation of COX-2 expression, in which several consensus sites in the COX-2 promoter have been identified as regulatory sequences for COX-2 induction in response to various stimuli in various cells. In osteoblasts, NF-κB, NF-IL6, AP-1, C/EBP-α, -β, CRE and Runx2 are known to be involved in the transcriptional induction of COX-2 (Yamamoto et al., 1995; Harrison et al., 2000; Okada et al., 2000b; Chikazu et al., 2002). Regarding mPGES, however, although the structure of the human gene, including a 632-bp 5′-flanking region, has been reported (Forsberg et al., 2000), transcription factors or transcriptional regulatory elements have been studied little. Our colleagues recently reported that the binding of Egr-1, an inducible transcription factor, to the proximal GC box is an essential event that directs the regulatory

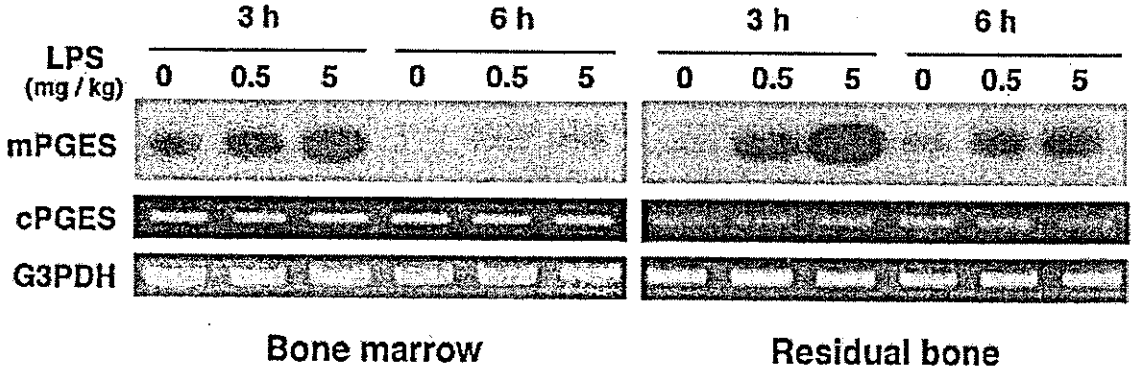

Fig. 3. Effect of intraperitoneal injection of LPS on mPGES and cPGES mRNA levels in bone marrow and the residual bone. After 3 and 6 h the intraperitoneal injection of PBS (0) or LPS (0.5 and 5 mg/kg) to mice, mRNA was extracted separately from the bone marrow of long bones and the residual bone. mPGES and cPGES mRNA levels were determined by RT-PCR/Southern blotting and RT-PCR, respectively.

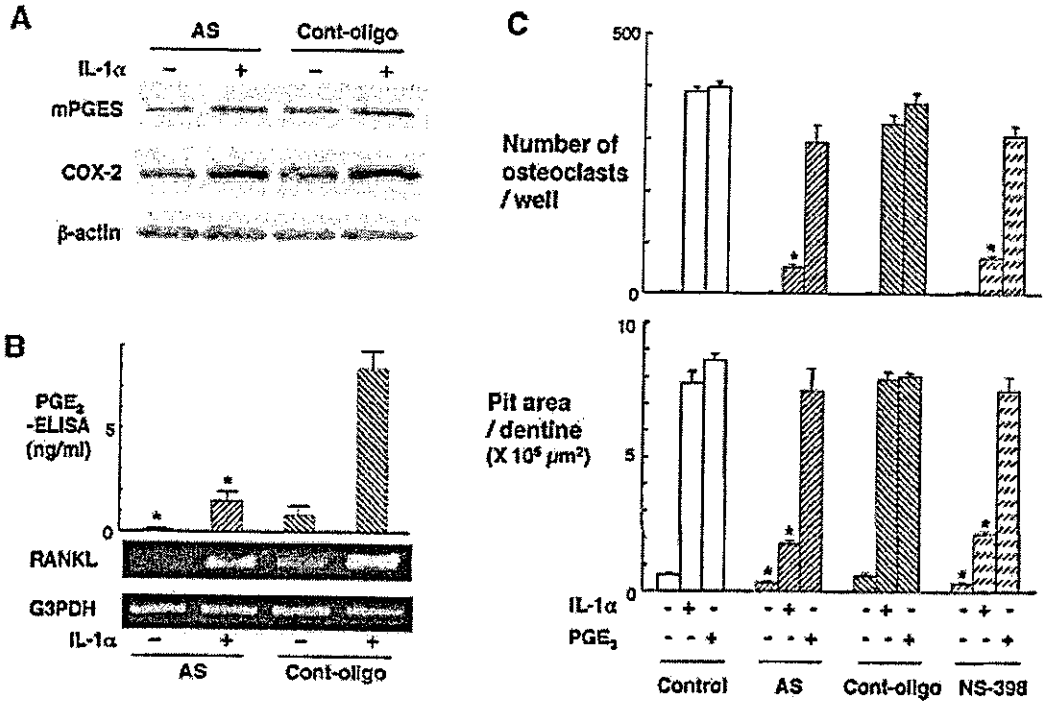

Fig. 4. Inhibitory effects of an mPGES antisense oligonucleotide on mPGES expression (A), PGE_2 production and RANKL expression (B), and osteoclastic bone resorption (C). A: Effects of the antisense and the control oligonucleotides on mPGES and COX-2 protein levels determined by Western blotting in the primary osteoblast culture with and without IL-1α (1 ng/ml) stimulation for 12 h. B: Effects of the antisense and control oligonucleotides on medium PGE_2 level and RANKL mRNA level measured by ELISA and semiquantitative RT-PCR, respectively, in the primary osteoblast culture with and without IL-1α stimulation. C: Effects of the oligonucleotides and NS-398, a specific COX-2 inhibitor, on osteoclastogenesis and resorbed pit formation on the dentine slice determined as described above (Fig. 1) in the coculture with and without IL-1α or PGE_2. These oligonucleotides and NS-398 were first added to cultured primary osteoblasts, and after 4 h, cocultured with bone marrow cells with and without each agent. $^*P < 0.01$, significant inhibition from the control-oligonucleotide culture (B) and from the control culture (C). Data are expressed as means (bars) ± SEMs (error bars) for eight cultures/group.

expression of mPGES under proinflammatory stimulations by LPS, IL-1, and TNF-α in mouse osteoblastic MC3T3-E1 cells (Naraba et al., 2002). Although the mouse mPGES promoter contains several other consensus binding sites such as C/EBP-α, -β, and AP-1, which have been implicated in COX-2 induction, the report failed to show the involvement of these sites in the promoter activation. Since there was no binding site for NF-κB, NF-IL6, CRE or Runx2 in the mPGES promoter, transcriptional mechanisms for inducible expression of mPGES and COX-2 are likely to be distinct. In addition, the time course of the stimulation of protein levels of mPGES and COX-2 by bone resorptive cytokines was different: the former kept increasing during the culture periods while the latter was transient with the peak around 3–6 h. This discrepancy also implies a difference in translational or post-translational regulations between mPGES and COX-2 by these cytokines. Even though both enzymes are stimulus-inducible and function sequentially in the same PGE_2-biosynthetic pathway, the kinetics of the induction seems not to be entirely identical in osteoblasts.

A synthesized antisense oligonucleotide inhibited osteoclastic bone resorption in the coculture of osteoblasts and marrow cells. We suspect that the target of this antisense oligonucleotide was osteoblasts because it inhibited RANKL expression in cultured primary osteoblasts. In this system, however, the possible involvement of the down-regulation of mPGES in bone marrow hemopoietic cells that are osteoclast precursors in this effect cannot be denied. In fact, mPGES is reported to be expressed and up-regulated transcriptionally by proinflammatory cytokines in the macrophage cell line RAW264.7 (Naraba et al., 2002). Furthermore, previous studies showed that PGE_2 has a potency to stimulate osteoclast formation from precursors directly in the absence of osteoblasts/stromal cells (Wani et al., 1999; Li et al., 2000). The cellular mechanism of cytokine-induced osteoclastic bone resorption through mPGES induction and PGE_2 production still remains to be investigated.

It is expected that the mPGES pathway will be a target for therapeutic intervention for patients with bone resorptive diseases like postmenopausal osteoporosis and RA joint destruction. Bone resorptive cytokines used in this study are actually known to contribute to these disorders. We and others have reported that up-regulation of IL-1 and TNF-α production in bone marrow are implicated in bone loss with estrogen withdrawal at least partly through PGE_2 production (Kawaguchi et al., 1995c; Pacifici, 1996; Pfeilschifter et al., 2002). Although our preliminary studies so far have failed to detect the regulation of mPGES expression in bone or bone marrow by ovariectomy in mice, possibility of the involvement

of a subtle change of endogenous mPGES level in the etiology of postmenopausal osteoporosis cannot be ignored. We also reported that another cytokine FGF-2 in the synovial fluid plays a role in the RA joint destruction (Manabe et al., 1999) and that FGF-2 stimulates osteoclastogenesis through PGE_2 production in osteoblasts (Kawaguchi et al., 1995c, 2000; Chikazu et al., 2001). Since proinflammatory cytokines are reported to induce mPGES in synovial cells as well (Stichtenoth et al., 2001), mPGES might also possibly involved in the pathophysiology of the RA joint destruction. Unlike NSAIDs, which inhibit COX activity and suppress not only PGE_2 but also other essential prostanoids, which maintain physiological functions, an inhibitor of this PGE_2 specific enzyme could provide a highly selective treatment for these diseases with low side effects.

It should be noticed that the present study is limited to in vitro experiments. In fact, PGs, particularly those of the E series, are known to have potent effects not only on bone resorption, but also on bone formation in vivo (Miller and Marks, 1994; Jee and Ma, 1997). The osteogenic effects are mainly seen when a substantial amount of exogenous PGEs were applied locally or systemically. Regarding the role of endogenous PGEs, recent reports on knockout mice of PGEs-related molecules including PGE_2 receptors or COX-2 failed to demonstrate their abnormalities of skeletal development or growth, indicating that endogenous PGEs are not important for physiologic osteogenesis; however, under pathologic conditions such as fracture healing and mechanical stimulation, osteogenesis is reported to be impaired by the deficiency of COX-2 and EP2, respectively (Akhter et al., 2001; Simon et al., 2002). Contrarily, studies on knockout mice have also shown the essential role of COX-2 and EP4 in the stimulation of bone resorption by parathyroid hormone and LPS in vivo (Sakuma et al., 2000; Okada et al., 2000a). Hence, further studies using mPGES-deficient mice will be needed to clarify the in vivo roles of endogenous mPGES in bone formation and resorption under physiologic and pathologic conditions.

LITERATURE CITED

Akatsu T, Takahashi N, Debaki K, Morita I, Murota S, Nagata N, Takatani O, Suda T. 1989. Prostaglandins promote osteoclastlike cell formation by a mechanism involving cyclic adenosine 3′,5′-monophosphate in mouse bone marrow cell cultures. J Bone Miner Res 4:29–35.

Akatsu T, Takahashi N, Udagawa N, Imamura K, Yamaguchi A, Sato K, Nagata N, Suda T. 1991. Role of prostaglandins in interleukin-1-induced bone resorption in mice in vitro. J Bone Miner Res 6:183–189.

Akhter MP, Cullen DM, Gong G, Recker RR. 2001. Bone biomechanical properties in prostaglandin EP1 and EP2 knockout mice. Bone 29:121–125.

Chikazu D, Katagiri M, Ogasawara T, Ogata N, Shimoaka T, Takato T, Nakamura K, Kawaguchi H. 2001. Regulation of osteoclast differentiation by fibroblast growth factor 2: Stimulation of receptor activator of nuclear factor kappaB ligand/osteoclast differentiation factor expression in osteoblasts and inhibition of macrophage colony-stimulating factor function in osteoclast precursors. J Bone Miner Res 16:2074–2081.

Chikazu D, Li X, Kawaguchi H, Sakuma Y, Voznesensky OS, Adams DJ, Xu M, Hoshio K, Katavic V, Herschman HR, Raisz LG, Pilbeam CC. 2002. Bone morphogenetic protein 2 induces cyclo-oxygenase 2 in osteoblasts via a Cbfal binding site: Role in effects of bone morphogenetic protein 2 in vitro and in vivo. J Bone Miner Res 17: 1430–1440.

Filion F, Bouchard N, Goff AK, Lussier JG, Sirois J. 2001. Molecular cloning and induction of bovine prostaglandin E synthase by gonadotropins in ovarian follicles prior to ovulation in vivo. J Biol Chem 276:34323–34330.

Forsberg L, Leeb L, Thoren S, Morgenstern R, Jakobsson P. 2000. Human glutathione dependent prostaglandin E synthase: Gene structure and regulation. FEBS Lett 471:78–82.

Fry DE, Pearlstein L, Fulton RL, Polh HC Jr. 1980. Multiple system organ failure. The role of uncontrolled infection. Arch Surg 115: 136–140.

Funk CD. 2001. Prostaglandins and leukotrienes: Advances in eicosanoid biology. Science 294:1871–1875.

Goldring SR, Schiller AL, Roelke M, Rourke CM, O'Neill DA. 1983. The synovial-like membrane at the bone-cement interface in loose total hip replacements and its proposed role in bone lysis. J Bone Joint Surg 65:575–584.

Han R, Tsui S, Smith TJ. 2002. Up-regulation of prostaglandin E_2 synthesis by interleukin-1beta in human orbital fibroblasts involves coordinate induction of prostaglandin-endoperoxide H synthase-2 and glutathione-dependent prostaglandin E_2 synthase expression. J Biol Chem 277:16355–16364.

Harris M, Jenkins MV, Bennet A, Wills MR. 1973. Prostaglandin production and bone resorption by dental cysts. Nature 245:213–215.

Harris SG, Padilla J, Koumas L, Ray D, Phipps RP. 2002. Prostaglandins as modulators of immunity. Trends Immunol 23:144–150.

Harrison JR, Kelly PL, Pilbeam CC. 2000. Involvement of CCAAT enhancer binding protein transcription factors in the regulation of prostaglandin G/H synthase 2 expression by interleukin-1 in osteoblastic MC3T3-E1 cells. J Bone Miner Res 15:1138–1146.

Harvey W, Guat-Chen F, Gordon D, Meghji S, Evans A, Harris M. 1984. Evidence for fibroblasts as the major source of prostacyclin and prostaglandin synthesis in dental cyst in man. Arch Oral Biol 29:223–229.

Horowitz SM, Rapuano BP, Lane JM, Burstein AH. 1994. The interaction of the macrophage and the osteoblast in the pathophysiology of aseptic loosening of joint replacements. Calcif Tissue Int 54:320–324.

Jakobsson PJ, Thoren S, Morgenstern R, Samuelsson B. 1999. Identification of human prostaglandin E synthase: A microsomal, glutathione-dependent, inducible enzyme, constituting a potential novel drug target. Proc Natl Acad Sci USA 96:7220–7225.

Jee WS, Ma YF. 1997. The in vivo anabolic actions of prostaglandins in bone. Bone 21:297–304.

Kawaguchi H, Raisz LG, Voznesensky OS, Alander CB, Hakeda Y, Pilbeam CC. 1994. Regulation of the two prostaglandin G/H synthases by parathyroid hormone, interleukin-1, cortisol, and prostaglandin E_2 in cultured neonatal mouse calvariae. Endocrinology 135:1157–1164.

Kawaguchi H, Pilbeam CC, Harrison JR, Raisz LG. 1995a. The role of prostaglandins in the regulation of bone metabolism. Clin Orthop 313:36–46.

Kawaguchi H, Pilbeam CC, Gronowicz G, Abreu C, Fletcher BS, Herschman HR, Raisz LG, Hurley MM. 1995b. Transcriptional induction of prostaglandin G/H synthase-2 by basic fibloblast growth factor. J Clin Invest 96:923–930.

Kawaguchi H, Pilbeam CC, Vargas SJ, Morse EE, Lorenzo JA, Raisz LG. 1995c. Ovariectomy enhances and estrogen replacement inhibits the activity of bone marrow factors that stimulate prostaglandin production in cultured mouse calvariae. J Clin Invest 96: 539–548.

Kawaguchi H, Nemoto K, Raisz LG, Harrison JR, Voznesensky OS, Alander CB, Pilbeam CC. 1996. Interleukin-4 inhibits prostaglandin G/H synthase-2 and cytosolic phospholipase A2 induction in neonatal mouse parietal bone cultures. J Bone Miner Res 11:358–366.

Kawaguchi H, Chikazu D, Nakamura K, Kumegawa M, Hakeda Y. 2000. Direct and indirect actions of fibroblast growth factor 2 on osteoclastic bone resorption in cultures. J Bone Miner Res 15:466–473.

Klein DC, Raisz LG. 1970. Prostaglandins: Stimulation of bone resorption in tissue culture. Endocrinology 86:1436–1440.

Li X, Okada Y, Pilbeam CC, Lorenzo JA, Kennedy CR, Breyer RM, Raisz LG. 2000. Knockout of the Murine Prostaglandin EP_2 Receptor Impairs Osteoclastogenesis in vitro. Endocrinology 141:2054–2061.

Manabe N, Oda H, Nakamura K, Kuga Y, Uchida S, Kawaguchi H. 1999. Involvement of fibroblast growth factor-2 in joint destruction of rheumatoid arthritis patients. Rheumatology 38:714–720.

Mancini JA, Blood K, Guay J, Gordon R, Claveau D, Chan CC, Riendeau D. 2001. Cloning, expression, and up-regulation of inducible rat prostaglandin e synthase during lipopolysaccharide-induced pyresis and adjuvant-induced arthritis. J Biol Chem 276: 4469–4475.

Miller SC, Marks SC Jr. 1994. Effects of prostaglandins on the skeleton. Clin Plast Surg 21:393–400.

Minkin C, Fredricks RS, Pokress S, Rude RK, Sharp CF Jr., Tong M, Singer FR. 1981. Bone resorption and humoral hypercalcemia of malignancy: Stimulation of bone resorption in vitro by tumor extracts is inhibited by prostaglandin synthesis inhibitors. J Clin Endocrinol Metab 53:941–947.

Murakami M, Naraba H, Tanioka T, Semmyo N, Nakatani Y, Kojima F, Ikeda T, Fueki M, Ueno A, Oh-Ishi S, Kudo I. 2000. Regulation of prostaglandin E_2 biosynthesis by inducible membrane-associated prostaglandin E_2 synthase that acts in concert with cyclooxygenase-2. J Biol Chem 275:32783–32792.

Naraba H, Yokoyama C, Tago N, Murakami M, Kudo I, Fueki M, Oh-Ishi S, Tanabe T. 2002. Transcriptional regulation of the membrane-associated prostaglandin E_2 synthase gene. Essential role of the transcription factor Egr-1. J Biol Chem 277:28601–28608.

Okada Y, Lorenzo JA, Freeman AM, Tomita M, Morham SG, Raisz LG, Pilbeam CC. 2000a. Prostaglandin G/H synthase-2 is required for maximal formation of osteoclast-like cells in culture. J Clin Invest 105:823–832.

Okada Y, Voznesensky O, Herschman H, Harrison J, Pilbeam CC. 2000b. Identification of multiple cis-acting elements mediating the induction of prostaglandin G/H synthase-2 by phorbol ester in murine osteoblastic cells. J Cell Biochem 78:197–209.

Pacifici R. 1996. Estrogen, cytokines, and pathogenesis of postmenopausal osteoporosis. J Bone Miner Res 11:1043–1051.

Pfeilschifter J, Koditz R, Pfohl M, Schatz H. 2002. Changes in proinflammatory cytokine activity after menopause. Endocr Rev 23: 90–119.

Pilbeam CC, Kawaguchi H, Hakeda Y, Voznesensky O, Alander CB, Raisz LG. 1993. Differential regulation of inducible and constitutive prostaglandin endoperoxide synthase in osteoblastic MC3T3-E1 cells. J Biol Chem 268:25643–25649.

Raisz LG. 1995. Physiologic and pathologic roles of prostaglandins and other eicosanoids in bone metabolism. J Ntr 125:2024S–2027S.

Raisz LG, Alander CB, Fall PM, Simmons HA. 1990. Effects of prostaglandin F_2 alpha on bone formation and resorption in cultured neonatal mouse calvariae: Role of prostaglandin E_2 production. Endocrinology 126:1076–1079.

Robinson DR, Tashjian AH Jr., Levine L. 1975. Prostaglandin-stimulated bone resorption by rheumatoid synovia. A possible mechanism for bone destruction in rheumatoid arthritis. J Clin Invest 56:1181–1188.

Sakuma Y, Tanaka K, Suda M, Komatsu Y, Yasoda A, Miura M, Ozaki A, Narumiya S, Sugimoto Y, Ichikawa A, Ushikubi F, Nakao K. 2000. Impaired bone resorption by lipopolysaccharide in vivo in mice deficient in the prostaglandin E receptor EP4 subtype. Infect Immun 68:6819–6825.

Satoh K, Nagano Y, Shimomura C, Suzuki N, Saeki Y, Yokota H. 2000. Expression of prostaglandin E synthase mRNA is induced in beta-amyloid treated rat astrocytes. Neurosci Lett 283:221–223.

Shinar G, Rodan GA. 1990. Biphasic effects of transforming growth factor-beta on the production of osteoclast-like cells in mouse bone marrow cultures: The role of prostaglandins in the generation of these cells. Endocrinology 126:3153–3158.

Simon AM, Manigrasso MB, O'Connor JP. 2002. Cyclo-oxygenase 2 function is essential for bone fracture healing. J Bone Miner Res 17: 963–976.

Smith WL, Langenbach R. 2001. Why there are two cyclooxygenase isozymes. J Clin Invest 107:1491–1495.

Soler M, Camacho M, Escudero JR, Iniguez MA, Vila L. 2000. Human vascular smooth muscle cells but not endothelial cells express prostaglandin E synthase. Circ Res 87:504–507.

Stichtenoth DO, Thoren S, Bian H, Peters-Golden M, Jakobsson PJ, Crofford L. 2001. Microsomal prostaglandin E synthase is regulated by proinflammatory cytokines and glucocorticoids in primary rheumatoid synovial cells. J Immunol 167:469–474.

Suda T, Takahashi N, Udagawa N, Jimi E, Gillespie MT, Martin TJ. 1999. Modulation of osteoclast differentiation and function by the new members of the tumor necrosis factor receptor and ligand families. Endocr Rev 20:345–357.

Tanioka T, Nakatani Y, Semmyo N, Murakami M, Kudo I. 2000. Molecular identification of cytosolic prostaglandin E_2 synthase that is functionally coupled with cyclooxygenase-1 in immediate prostaglandin E_2 biosynthesis. J Biol Chem 275:32775–32782.

Tashjian AH Jr., Voelkel EF, Levine L. 1977. Effects of hydrocortisone on the hypercalcemia and plasma levels of 13,14-dihydro-15-keto-prostaglandin E_2 in mice bearing the HSDM1 fibrosarcoma. Biochem Biophys Res Commun 74:199–207.

Tashjian AH Jr., Bosma TJ, Levine L. 1988. Use of minoxidil to demonstrate that prostacyclin is not the mediator of bone resorption stimulated by growth factors in mouse calvariae. Endocrinology 123:969–974.

Wani MR, Fuller K, Kim NS, Choi Y, Chambers T. 1999. Prostaglandin E_2 cooperates with TRANCE in osteoclast induction from hemopoietic precursors: Synergistic activation of differentiation, cell spreading, and fusion. Endocrinology 140:1927–1935.

Yamagata K, Matsumura K, Inoue W, Shiraki T, Suzuki K, Yasuda S, Sugiura H, Cao C, Watanabe Y, Kobayashi S. 2001. Coexpression of microsomal-type prostaglandin E synthase with cyclooxygenase-2 in brain endothelial cells of rats during endotoxin-induced fever. J Neurosci 21:2669–2677.

Yamamoto K, Arakawa T, Ueda N, Yamamoto S. 1995. Transcriptional roles of nuclear factor kappa B and nuclear factor-interleukin-6 in the tumor necrosis factor alpha-dependent induction of cyclooxygenase-2 in MC3T3-E1 cells. J Biol Chem 270:31315–31320.

Zimmermann M. 1983. Ethical guidelines for investigations of experimental pain in conscious animals. Pain 16:109–110.

Available online at www.sciencedirect.com
SCIENCE DIRECT®
Biomaterials 24 (2003) 4495–4506
Biomaterials
www.elsevier.com/locate/biomaterials

Polyion complex micelles from plasmid DNA and poly(ethylene glycol)–poly(L-lysine) block copolymer as serum-tolerable polyplex system: physicochemical properties of micelles relevant to gene transfection efficiency

Keiji Itaka[a,b], Kyosuke Yamauchi[a], Atsushi Harada[a], Kozo Nakamura[b], Hiroshi Kawaguchi[b], Kazunori Kataoka[a,*]

[a] *Department of Materials Science and Engineering, Graduate School of Engineering, The University of Tokyo, 7-3-1 Hongo, Bunkyo-ku, Tokyo 113-8656, Japan*

[b] *Department of Orthopaedic Surgery, Faculty of Medicine, The University of Tokyo, 7-3-1 Hongo, Bunkyo-ku, Tokyo 113-8655, Japan*

Abstract

Polyion complex (PIC) micelles composed of the poly(ethylene glycol)–poly(L-lysine) (PEG–PLL) block copolymer and plasmid DNA (pDNA) were investigated in this study from a physicochemical viewpoint to get insight into the structural feature of the PIC micellar vector system to show practical gene transfection efficacy particularly under serum-containing medium. The residual ratio (r) of the lysine units in PEG–PLL to the phosphate units of pDNA in the system significantly affects the size of the PIC micelles evaluated from dynamic light scattering, being decreased from approximately 120 to 80 nm with an increase in the r value for the region with $r \geqslant 1.0$. The zeta potential of the complexes slightly increased with r in the same region, yet maintained a very small absolute value and leveled off to a few mV at $r \approx 2.0$. These results suggest that the micelles are most likely to take the core-shell structure with dense PEG palisades surrounding the PIC core to compartmentalize the condensed pDNA. Furthermore, an increasing r value in the region of $r \geqslant 1$ induces a rearrangement of the stoichiometric complex formed at $r = 1.0$ to the non-stoichiometric complex composed of the excess block copolymer. The association number of pDNA and the block copolymer in the micelle was estimated from the apparent micellar molecular weight determined by static light scattering measurements, indicating that a single pDNA molecule was incorporated in each of the micelles prepared from the PEG ($M_w = 12{,}000$ g/mol)–PLL (polymerization degree of PLL segment: 48) (12-48) block copolymer at $r = 2.0$. These 12-48/pDNA micelles showed a gene expression comparable to the lipofection toward cultured 293 cells, though 100 μM chloroquine was required in the transfection medium. Notably, even in the presence of serum, the PIC micelles achieved appreciable cellular association to attain a high gene expression, which is in sharp contrast with the drastic decrease in the gene expression for lipoplex system in the presence of serum. A virus-comparable size (~100 nm) with a serum-tolerable property of the PIC micelles indeed suggests their promising feasibility as non-viral gene-vector systems used for clinical gene therapy.

Keywords: Gene vector; Poly(ethylene glycol)–poly(L-lysine) (PEG–PLL) block copolymer; Polyion complex; Micelle; Static light scattering; Zeta potential; Luciferase assay

Abbreviations: PIC, polyion complex; PEG–PLL, poly(ethylene glycol)–poly(L-lysine) block copolymer; Charge ratio (r), the residual molar ratio of L-lysine in PEG–PLL to phosphate in the plasmid DNA; pDNA, plasmid DNA; M_w, weight-averaged molecular weight; $M_{w,app}$, the apparent weight-averaged molecular weight; DP, degree of polymerization; ζ, zeta potential; DMEM, Dulbecco's modified eagle medium; FBS, fetal bovine serum; PLys-polyplex, poly(L-lysine)/DNA complex; lipoplex, polycationic lipid/DNA complex; EtBr, ethidium bromide; FRET, fluorescence resonance energy transfer; PBS, phosphate buffered saline; DLS, dynamic light scattering; SLS, static light scattering.

*Corresponding author. Tel.: +81-35841-7138; fax: +81-35841-7139.

E-mail address: kataoka@bmw.t.u-tokyo.ac.jp (K. Kataoka).

1. Introduction

The fast progress in clinical gene therapy has significantly motivated the development of safe and efficient non-viral gene delivery systems, which may substitute for viral vectors still having inherent safety problems such as immunogenicity and viral recombination [1]. Most non-viral systems so far applied are composed of cationic lipids or polymers that can be associated with negatively charged DNA, and the appreciable enhancement in gene expression has been

0142-9612/03/$ - see front matter © 2003 Elsevier Ltd. All rights reserved.
doi:10.1016/S0142-9612(03)00347-8

achieved by the use of these lipoplex and polyplex systems especially in in vitro transfection [2–6]. Nevertheless, serious problems still remain in these non-viral vector systems especially in an in vivo situation. Poor solubility of the complexes particularly for the charge-neutralized condition is one of major problems. Excess cationic components in the complexes may improve the solubility, yet the positively charged nature of the complexes induces other problems such as cytotoxicity and the non-specific disposition to medium components.

These problems may be overcome by introduction of a hydrophilic segment onto the surface of the complexes. In this regard, polyplex systems based on block- or graft-catiomers with neutral and hydrophilic segments, such as poly(ethylene glycol) (PEG), are particularly attractive, because they may form a characteristic micelle structure with a hydrophilic shell layer surrounding the core of the polyion complex (PIC) formed between DNA and the catiomer segments (PIC micelles) [7–13]. Indeed, the PIC micellar vector composed of poly(ethylene glycol)–poly(L-lysine) (PEG–PLL) block copolymers exhibited improved solubility even under a charge-neutralized condition [10,14–17]. Furthermore, there was observed a remarkable increase in the nuclease resistance of the micelle-entrapped pDNA [18]. The practical advantage of this system is the excellent stability in a serum-containing medium [19], lending itself to be useful for gene delivery under physiological circumstances.

The chemical structure and composition of the constituent block catiomers definitely affect the physicochemical properties of the PIC micelles, including their architecture, size, and stability, and thus are likely to be crucial parameters for determining their gene transfection efficiency. Although a few studies in this regard have so far been reported [8,20,21], a general consensus on the structure–function relationship of PIC micellar vector system has not yet been accomplished. This led us to the present study to thoroughly investigate the structure–function relationship of PIC micellar vector systems based on PEG–PLL, featuring their utility as gene transfection systems especially under serum-containing conditions.

2. Materials and methods

2.1. Materials

Three types of PEG–PLL block copolymers (PEG–PLL; PEG $M_w = 12{,}000$ g/mol) having different polymerization degrees of the PLL segments (7, 19, 48; the code names are 12-7, 12-19, 12-48, respectively) were synthesized as previously reported [10]. Poly(L-lysine) with a degree of polymerization(DP) = 258 was purchased from the Sigma Chemical Co. LipofectAMINE™ reagent was purchased from Gibco-BRL (Burlington, USA). Plasmid DNA (pDNA) encoding luciferase (pGL3-Luc, Promega; 5,256 bps) was amplified in competent DH5α *Escherichia coli* and purified using EndoFree™ Plasmid Maxi or Mega Kits (QIAGEN, Germany). The DNA concentration was determined by reading the absorbance at 260 nm. Dulbecco's modified eagle medium (DMEM) and fetal bovine serum (FBS) were purchased from Sigma.

2.2. Preparation of polyion complex micelles and other complexes

The PEG–PLL block copolymer and pDNA were separately dissolved in 10 mM Tris-HCl buffer (pH 7.4). Both solutions were mixed at various charge ratios of the number of lysine units per nucleotide (r = [lysine residue]/[nucleotide]). The poly(L-lysine)/DNA complex (PLys-polyplex) was similarly prepared by mixing poly(L-lysine) in the pDNA solution. The cationic lipid/DNA complex (lipoplex) was prepared by mixing the pDNA solution and LipofectAMINE™ reagent following the protocol provided by the manufacturer. In all cases except for the evaluation of the critical association concentration, the final DNA concentration was adjusted to 30 μg/ml.

2.3. Light scattering measurements

The light scattering measurements were carried out using a DLS-7000 (Otsuka Electronics Co., Ltd., Osaka, Japan). A vertically polarized light of 488 nm wavelength from an Ar ion laser (75 mW) was used as the incident beam. All measurements were carried out at 25.0°C.

During the dynamic light scattering (DLS) measurements, the autocorrelation function was developed by the following equation:

$$g^{(1)}(\tau) = \exp[-\bar{\Gamma}\tau + (\mu_2/2)\tau^2 - (\mu_3/3!)\tau^3 + \cdots] \quad (1)$$

yielding an average characteristic line width of $\bar{\Gamma}$ The z-averaged diffusion coefficient was obtained from $\bar{\Gamma}$ based on the following equations:

$$\bar{\Gamma} = Dq^2, \quad (2)$$

$$q = (4\pi n/\lambda)\sin(\theta/2), \quad (3)$$

where q is the magnitude of the scattering vector, n is the refractive index of the solvent, λ is the wavelength of the incident beam, and θ is the detection angle. The hydrodynamic diameter d_h can then be calculated using the Stokes–Einstein equation:

$$d_h = k_B T/(3\pi\eta D), \quad (4)$$

where k_B is the Boltzmann constant, T is the absolute temperature, and η is the viscosity of the solvent. Also,

the polydispersity index ($PI = \mu_2/\bar{\Gamma}^2$) was derived from Eq. (1).

During the static light scattering (SLS) measurements, the light scattered by a dilute polymer solution may be expressed by the following equation:

$$KC/\Delta R(\theta) = (1/M_{w,app})(1 + q^2R_g^2/3) + 2A_2C, \quad (5)$$

where C is the concentration of the polymer, $\Delta R(\theta)$ is the difference between the Rayleigh ratio of the solution and that of the solvent, $M_{w,app}$ is the apparent weight-averaged molecular weight, R_g^2 is the mean square radius of gyration, A_2 is the second virial coefficient, and $K = (4p^2n^2(dn/dc)^2)/(N_A l^4)$ (N_A is Avogadro's number). The known Rayleigh ratio of benzene was used as the calibration standard.

For each sample, the angular dependence of $\Delta R(\theta)$ was measured, and the change in $M_{w,app}$ with the mixing charge ratio (r) was evaluated using the Debye equation as follows:

$$KC/\Delta R(0) = 1/M_{w,app} + 2A_2C. \quad (6)$$

The increments of the refractive index, dn/dc, of the solutions were measured using a DRM-1020 double-beam differential refractometer (Otsuka Electronics Co., Ltd., Osaka, Japan).

2.4. Exclusion assay of ethidium bromide

PIC micelle solutions with various mixing charge ratios and ethidium bromide (EtBr) solution were separately prepared and then mixed. The final concentration was adjusted to 1.43 μg/ml of pDNA and 1.7 μg/ml of EtBr. The mixtures were stored overnight in the dark followed by the fluorescence intensity measurement at 25°C (λ_{ex} 527 nm, λ_{em} 585 nm) using a spectrofluorometer (JASCO, FP-777).

2.5. Evaluation of the condensation state of pDNA by fluorescence resonance energy transfer

Fluorescence resonance energy transfer (FRET) measurements of complexes containing doubly labeled pDNA were performed in a similar way as that previously described [19]. Briefly, pDNA was labeled using a Label IT Nucleic Acid Labeling Kit (Panvera, USA). Following a protocol provided by the manufacturer, slightly modified to allow double labeling of DNA, 5–50 μl of a pDNA solution (1 mg/ml) and the same amount of Label IT Reagent (for fluorescein or X-rhodamine) were mixed in 20 mM MOPS buffer (pH 7.5) and incubated at 37°C for 2 h. For double labeling of the fluorescein and X-rhodamine, the two reagents were simultaneously added to the pDNA solution. Unreacted labeling reagent was removed and pDNA was purified by ethanol precipitation.

Fluorescence emission of the free pDNA and DNA-loaded complex particles were measured at 25°C using a spectrofluorometer (JASCO, FP-777). The excitation wavelength was 492 nm.

2.6. Laser-Doppler electrophoresis measurements

Laser-Doppler electrophoresis measurements were carried out using a LEZA-600 (Otsuka Electronics Co., Ltd., Osaka, Japan) at 25.0°C. From the obtained electrophoretic mobility, the zeta potential (ζ) was calculated using the Smoluchowski equation as follows:

$$\zeta = 4\pi\eta u/\varepsilon, \quad (7)$$

where u is the electrophoretic mobility, η is the viscosity of the solvent, and ε is the dielectric constant of the solvent.

2.7. In vitro transfection

293 cells were seeded in six-well culture plates. After a 48 h incubation in medium containing 10% FBS, the cells were rinsed and then 1000 μl culture medium without FBS was added to each well. Complex solution (100 μl) (pDNA concentration was 30 μg/ml) was applied to each well. For the PIC micelles and PLL/pDNA complexes, 100 μM of chloroquine (Sigma) was included. After 4 h, the medium was removed and replaced by 10% FBS containing medium. After a further 24 h of incubation, the luciferase gene expression was measured. For the preincubation study with serum, medium containing 20 vol% FBS was added to the solutions of the complexes and incubated at 37°C for 30 min prior to the transfection study.

2.8. Analysis of cellular association of complexes

pDNA was labeled with fluorescein as previously described (2.5). The complexes (PIC micelles, PLys-polyplex, and lipoplex) loaded with fluorescein-labeled pDNA were applied to the 293 cells in a way similar to the procedure for in vitro transfection (2.7). After an hour of incubation, the culture medium was aspirated and cells were washed twice with phosphate buffered saline (PBS). After detachment by pipetting and resuspension in PBS, the cells were analyzed using a flow cytometer (EPICS XL, Beckman Coulter, Inc). Mock transfection allowed the definition of the natural fluorescence limit for the 293 cells and thus assessment of the fluorescein-positive cells. The cytometric data were analyzed using EXPO32™ software (Beckman Coulter, Inc).

3. Results and discussion

3.1. Evaluation of the size of PIC micelles by dynamic light scattering

As the size of the vector systems is known to be one of the crucial factors affecting their gene expression efficiency [11,22–25], the average diameter of the PIC micelles from pDNA and PEG–PLL with varying composition (12-7, 12-19, 12-48) was evaluated in detail using DLS in 10 mM Tris-HCl buffer (pH = 7.4). The mixing charge ratio (r), the residual molar ratio of the lysine units in PEG–PLL to phosphate units in pDNA in the mixture, was systematically changed in the range of $r = 0.4$–5.0, revealing the r-dependent change in the cumulant diameter of PEG–PLL/pDNA micelles as seen in Fig. 1(A). Also, the values of μ^2/Γ^2 (polydispersity index) were calculated and plotted in Fig. 1(B) to estimate the dispersity of each system.

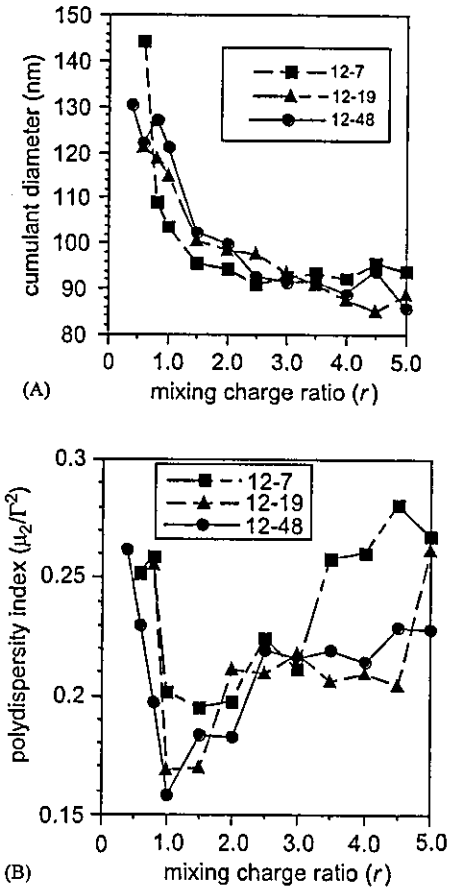

Fig. 1. (A) Change in the cumulant diameter with mixing charge ratio (r) for PIC micelles formed from pDNA and PEG–PLL (■, 12-7/pDNA; ▲, 12-19/pDNA; and ●, 12-48/pDNA). (B) Change in the polydispersity index (μ^2/Γ^2) with mixing charge ratio (r) for PIC micelles formed from pDNA and PEG–PLL (■, 12-7/pDNA; ▲, 12-19/pDNA; and ●, 12-48/pDNA).

Enough photon counts to determine the diffusion coefficient, and eventually the average diameter, were obtained for the samples with $r > 0.4$, suggesting the formation of PIC micelles in this region. There was observed a clear decrease in the diameter as r approaches unity with a concomitant decrease in the polydispersity index to less than 0.2, suggesting a narrowing of the complex distribution. A typical histogram profile in gamma-distribution mode of PIC micelles from pDNA/12-48 at $r = 1.0$ is shown in Fig. 2, demonstrating the feature of unimodal distribution of this system.

Worth noticing is the continuous decrease in the diameter even in the region with excess PEG–PLL ($r > 1.0$), followed by a leveling-off to approximately 90–100 nm at $r \approx 2.0$. It should be noted that several studies on the complexation of DNA with polycations, including block ionomers, revealed the coil–globule transition of DNA molecules upon complexation to take the compact conformation [26–29]. This process is called compaction or condensation, and in particular, was confirmed for the PEG–PLL/DNA system by various methods, including thermal analysis (salmon DNA) [15], dye-exclusion assay (calf thymus DNA) [30], and atomic-force microscopy (pDNA with 6 kbp) [17]. Thus, the decreased diameter of PEG–PLL/pDNA shown in Fig. 1 with an increase in the r value is likely to reflect the process of DNA condensation induced by the complexation with PEG–PLL. This process of DNA condensation can be evaluated from a change in the fluorescence intensity of the intercalating dye, such as EtBr, because EtBr is excluded from the double-helical strand of DNA with progress of the DNA condensation, resulting in a decreased fluorescent intensity (dye-exclusion assay).

The result of the dye-exclusion assay is shown in Fig. 3. In line with a trend in the diameter change with r as shown in Fig. 1(A), the fluorescent intensity of EtBr decreased with r, and leveled off at around $r \approx 2.0$, indicating that the pDNA condensation is completed at

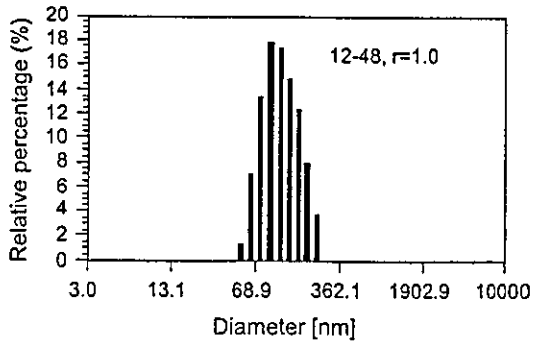

Fig. 2. Size distribution obtained from histogram analysis of DLS. A PIC micelle was formed from PEG–PLL(12-48) and pDNA at the mixing charge ratio (r) = 1.0.

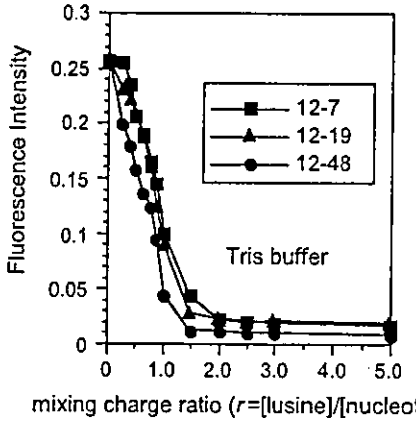

Fig. 3. Change in the fluorescence intensity of ethidium bromide with mixing charge ratio (r) for PIC micelles formed from pDNA and PEG–PLL (10 mM Tris, pH7.4) (■, 12-7/pDNA; ▲, 12-19/pDNA; and ●, 12-48/pDNA).

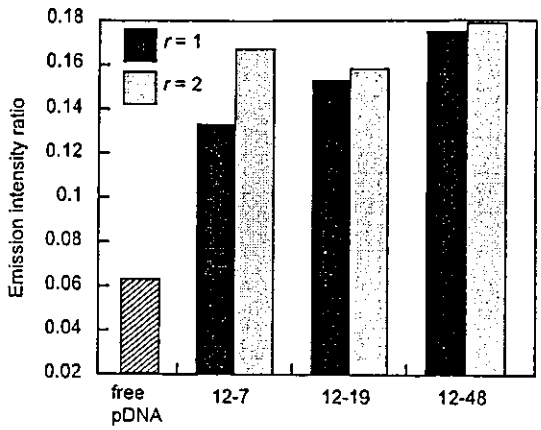

Fig. 4. FRET efficiency of X-rhodamine/fluorescein-labeled pDNA entrapped in PIC micelles made from PEG–PLL with varying compositions (12-7, 12-19, and 12-48) at different mixing charge ratios ($r = 1.0$ and 2.0).

this point. This is a striking contrast with the result of the dye-exclusion assay for linear DNA (calf thymus) complexation with PEG–PLL (10–78) reported by Seymour et al. [17], where the condensation was already completed at a stoichiometric mixing ratio ($r = 1.0$). Indeed, a similar tendency was observed for our system utilizing the linealized pDNA (data not shown). Native pDNA is in a super-coiled circular form, which certainly has a higher molecular restraint than the linear-formed DNA, and it is likely that these differences in molecular topology may crucially affect the condensation process of the DNA molecules. Presumably, ion-pair formation between the phosphate in pDNA and the protonated amino group in the PLL segment of PEG–PLL may not be completed at the stoichiometric charge ratio due to the steric reason, requiring excess PLL strands to participate in the ion-pair formation with residual phosphate groups in the pDNA strands to promote further condensation. Eventually, size reduction as well as dye exclusion accompanied with pDNA condensation were completed in the region with an excess equivalent of PEG–PLL.

Further investigations into the effect of the length of the PLL strands on pDNA condensation were then carried out by FRET measurement. PEG–PLL with varying PLL lengths (12-7, 12-19, 12-48) and doubly labeled (fluorescein and X-rhodamine) pDNA solutions were mixed at $r = 1.0$ and 2.0, respectively. The condensation state of pDNA inside the complex was evaluated by FRET between fluorescein (donor) and X-rhodamine (acceptor), typically represented by the emission intensity ratio of 597 nm (X-rhodamine emission) to 520 nm (fluorescein emission). As seen in Fig. 4, PEG–PLL with a longer PLL segment showed a higher emission intensity ratio at $r = 1.0$, indicating progressive condensation of pDNA in the micelle with a longer PLL segment. The ratios further increased with the r value and became almost equivalent for these three samples with different PLL length, which is consistent with the result of the dye-exclusion assay shown in Fig. 3. An appreciable increase in the emission intensity ratio with the r value for 12-7 suggests that an excess cationic component may be required for the block copolymer with a shorter PLL length to induce an effective condensation of pDNA.

Consequently, a decrease in the average diameter of the PIC micelles with an increase in the r values is indeed correlated with the pDNA condensation due to the complexation with PEG–PLL. Nevertheless, a significant decrease in the average diameter (121–80 nm) in the region of $1.0 \leqslant r \leqslant 2.0$ is unlikely to be explained only by the progress of the pDNA condensation. It is reasonable to assume that there might be a concomitant decrease in the association number, i.e., a decrease in the number of pDNA molecules included in each PIC micelle in this transient region of r between 1.0 and 2.0. This issue will be discussed later based on the results of the SLS in the PIC micelle systems (Section 3.3).

3.2. Zeta potential measurements of PIC micelles

In order to estimate the surface localization of the hydrophilic PEG segments in the PIC micelles, the zeta potential of the complexes was determined from laser-Doppler electrophoresis measurements. Measurement of the zeta potentials of the PEG–PLL/pDNA system with varying compositions revealed the existence of two regions with a boundary at $r = 1.0$, which may reflect a substantial difference in the property of the complexes. As shown in Fig. 5, in the region of $r < 1.0$, there was clearly observed two fractions having different zeta potential values: fractions with $\zeta = 0$ and $\zeta < 0$. The fraction with $\zeta < 0$ gradually shifted toward $\zeta = 0$ with r reaching unity, and merged with the other neutral

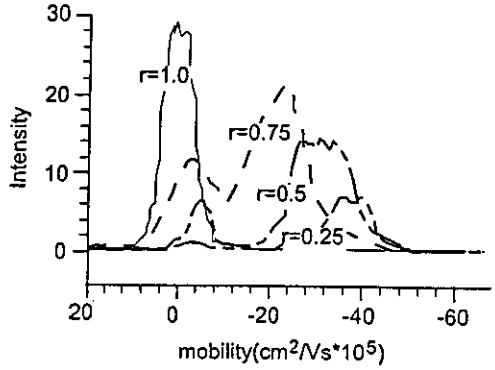

Fig. 5. Electropherogram of the 12-48/pDNA system for various mixing charge ratios (r).

fraction ($\zeta = 0$) at $r = 1.0$. The co-existence of two fractions at $r < 1.0$ suggests the cooperative nature of the complexes, leading to the formation of a stoichiometric complex fraction ($\zeta = 0$) (PIC micelles) even in the region with excess pDNA ($r < 1.0$). It should be noted that a similar co-operativity was also suggested for the complexation of PEG–PLL with linear salmon DNA based on thermal analysis results [15]. In general, cooperative complexation from a pair of oppositely charged polyelectrolytes is known to be observed for the system accompanying phase separation [26–29], which is indeed in line with the coil–globule transition (condensation) of DNA molecules upon complexation with PEG–PLL.

Worth noting is that an electorophoregram with enough intensity was not able to be obtained for the complex between pDNA and poly(L-lysine) with a chain length corresponding to the PLL segment of PEG–PLL used in this study (DP = 7–48) because the complexes were not stable enough to tolerate the applied electric field, and dissociated during the laser-Doppler electrophoresis measurement. This result clearly indicates that PEG segments in PEG–PLL play a substantial role in the increased stabilization of the complexes formed from PEG–PLL/pDNA. Presumably, the relatively low dielectric constant of the PEG palisade surrounding the complexed pDNA with PLL segment may contribute to increasing the complex stability. It should be noted that the coil–globule transition of DNA molecules is facilitated in the medium containing a high concentration of PEG due to the decreased dielectric constant [31].

On the other hand, the fraction with a negative zeta potential ($\zeta < 0$) is the non-stoichiometric complex consisting of partially neutralized pDNA with PEG–PLL, which diminishes at $r = 1.0$ because at this point, all the pDNA molecules should participate in the formation of stoichiometric PIC micelles with $\zeta = 0$. The stoichiometric PIC micelles at $r = 1.0$ existed as a clear solution without any precipitation for more than a month even though their zeta potentials were almost zero. Apparently, this is due to the formation of PEG palisades surrounding the micelle surface, ensuring the high solubility based on the steric stabilization propensity of the PEG layer.

Fig. 6(A) shows the change in the zeta potential with r values for PIC micelles having different PLL segment lengths. In all cases, there was observed two fractions in the region of $r < 1.0$, indicating the co-existence of two kinds of complexes, i.e., stoichiometric ($\zeta = 0$) and non-stoichiometric ($\zeta < 0$). A fraction of the non-stoichiometric complexes was merged into the stoichiometric fraction with r reaching unity. These results are consistent with a trend in the polydispersity factor shown in Fig. 1(B), in which the dispersity of the system gradually improves and becomes narrower with r approaching unity.

The zeta potential of the PIC micelles maintained a very small absolute value even in the region of $r \geqslant 1.0$, yet, as shown in Fig. 6(B) with a magnified y-axis, there was observed a slight increase in the zeta potential with an increase in the r value, reaching a plateau value of approximately 2–6 mV depending on the PLL chain length. These gradual changes in the zeta potential with r are in line with the average diameter profile observed

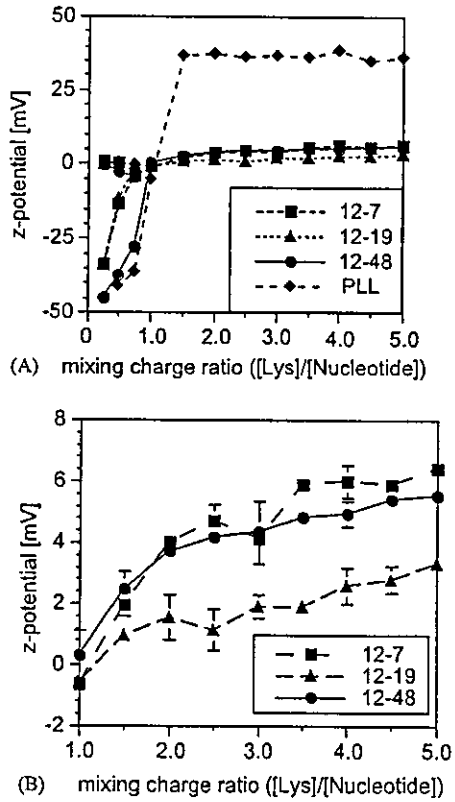

Fig. 6. (A) Change in the zeta potential with mixing charge ratio (r) for PIC micelle formed from pDNA and PEG–PLL (12-7, 12-19, 12-48) or PLL. (B) An enlarged form of (A). ■, 12-7/pDNA; ▲, 12-19/pDNA; ●, 12-48/pDNA; and ♦, PLL.

by DLS (Fig. 1) as well as with the pDNA condensation profile estimated by the dye-exclusion assay (Fig. 3). The most reasonable model to explain these trends is that, in the presence of an excess block copolymer, stoichiometric PIC micelles formed at $r = 1.0$ may undergo further rearrangement with a progressive pDNA condensation and a decreased association number to form the non-stoichiometric micelles composed of an excess block copolymer.

3.3. Static light scattering measurement of PEG–PLL/pDNA micelles

Further details of the PEG–PLL association with pDNA were then explored through measurement of the SLS of the system with a changing r value. It should be noted that the value of the reflective index increment (dn/dc) should be needed to estimate the apparent molecular weight ($M_{w,app}$) of the complex from SLS because K in Eq. (6) is a function of dn/dc. The dn/dc of the multicomponent system like the multimolecular complexes of the block copolymer as examined here may be expressed as a summation of the dn/dc of each component:

$$(dn/dc) = W_A(dn/dc)_A + W_B(dn/dc)_B + W_C(dn/dc)_C + \cdots, \quad (8)$$

where $(dn/dc)_A$, $(dn/dc)_B$, $(dn/dc)_C$, ... are the reflective index increments and W_A, W_B, W_C, ... are the weight fractions of the A, B, and C, ... components, respectively. To confirm the validity of Eq. (8) in the present case of the PEG–PLL/pDNA micelles, $(dn/dc)_{calc}$ for the micelles with varying r were calculated from Eq. (8) using the observed values of the refractive index increments of each component, $(dn/dc)_{PEG-PLL}$ and $(dn/dc)_{pDNA}$, which are summarized in Table 1, and then, compared with the experimental values ($(dn/dc)_{exp}$) of the micelles as seen in Table 2. Obviously, $(dn/dc)_{exp}$ nicely agreed with $(dn/dc)_{calc}$, indicating that Eq. (8) is applicable for the evaluation of the present system.

The values of $KC/\Delta R(0)$ were then measured in the region of 0.9–30 μg/ml of pDNA, and plotted in Fig. 7. Obviously, these values remained constant in this concentration range, indicating that a critical association phenomenon was not observed in a highly diluted condition as low as 0.9 μg/ml. Thus, $M_{w,app}$ was directly calculated from the Debye plots without taking into account the critical association concentration. The $M_{w,app}$ of each micelle with varying r value was then calculated based on Eq. (6), assuming that all of the components in the medium, both PEG–PLL and pDNA, participated in the micelle formation, and thus, the total concentration of PEG–PLL and pDNA was adopted as C in Eq. (6). As seen in Fig. 8, $M_{w,app}$ monotonously increased with an increased r value in the range of $r < 1.0$. This is consistent with an increase in the fraction of stoichiometric PIC micelle observed in the aforementioned zeta potential measurements (Section 3.2), and eventually at the neutralized condition of

Table 1
The dn/dc values of pDNA and PEG–PLL block copolymers

	pDNA	12-7	12-19	12-48
dn/dc	0.3331857	0.1438473	0.1471704	0.152084

Table 2
The dn/dc values of PIC micelles formed from pDNA and PEG–PLL block copolymer with various mixing charge ratio (r)

r(=[Lys]/[nucleotide])		0.6	1.0	2.0	5.0
$(dn/dc)_{cal}$	12-7	0.19190273	0.17593855	0.16137863	0.15127234
	12-19	0.22211613	0.20077711	0.17848611	0.16110413
	12-48	0.25050884	0.22754304	0.19974234	0.17472171
$(dn/dc)_{exp}$	12-7	0.1944355	0.1884075	0.1600874	0.1534566
	12-19	0.225735	0.206615	0.1861209	0.1693673
	12-48	0.243308	0.2252582	0.202066	0.1683278

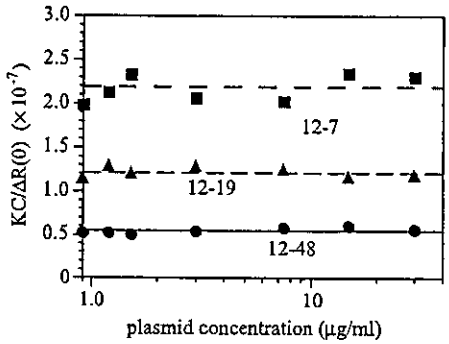

Fig. 7. Change in $KC/\Delta R(0)$ value with the concentration for PEG–PLL/pDNA system at $r = 1.0$. ■, 12-7/pDNA; ▲, 12-19/pDNA; and ●, 12-48/pDNA.

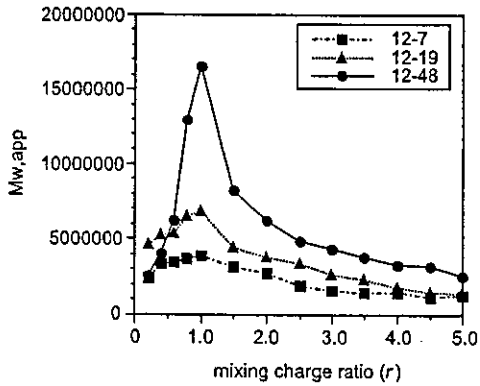

Fig. 8. Change in the apparent molecular weight ($M_{w,app}$) with mixing charge ratio (r) for PIC micelles formed from pDNA and PEG–PLL. ■, 12-7/pDNA; ▲, 12-19/pDNA; and ●, 12-48/pDNA.

Table 3
Mass per charge of PEG–PLL block copolymers

PEG–PLL	12-7	12-19	12-48
Mass per charge	1593	803	455

$r = 1.0$, $M_{w,app}$ should directly give that of the stoichiometric PIC micelles. Apparently, $M_{w,app}$ was maximized at $r = 1.0$ for all combinations with a pronounced trend as the length of the PLL segment increased. There was no further agglomeration of the complexes at $r = 1.0$, keeping a stable dispersion with a constant diameter for a prolonged period of storage, even though the absolute value of their zeta potential is almost zero.

It is noteworthy that $M_{w,app}$ of the associate correlates with the length of the PLL segment in the block copolymer. As expected from the mass per charge value of each PEG–PLL in Table 3, the weight ratio of PEG in the stoichiometric PIC micelle at $r = 1.0$ should inversely correlate to the PLL chain length of PEG–PLL. Indeed, the weight fractions of the PEG segments for the stoichiometric micelles composed of 12-7, 12-19, 12-48 were calculated to be 72, 53, 32 wt%, respectively, showing that micelles with a higher PEG content results in a lower $M_{w,app}$ or lower association number. The pDNA used here consists of 5256 bps, corresponding to ca. 3.4×10^6 g/mol. As calculated from the $M_{w,app}$ of micelles, an average number of two pDNA molecules may then be involved in each 12-48/pDNA micelle at $r = 1.0$. On the other hand, the association number of pDNA in the micelle is estimated to be unity for the 12-7/pDNA and 12-19/pDNA systems, assuming the formation of stoichiometric micelles. Presumably, the increased weight fraction of the PEG segment in the block copolymer with a shorter PLL chain may further contribute to segregate the PIC phase in the micelle from the aqueous exterior, allowing a single plasmid complex to stabilize without any secondary coalescence.

There is a clear and steep decrease in $M_{w,app}$ with an increased r value for the 12-48/pDNA system particularly in the region of $1.0 < r < 2.0$, suggesting a decreased association number. Assuming that all of the PEG–PLL molecules in the solution may participate in the micelle formation with pDNA, the association number of pDNA in the 12-48/pDNA micelle is calculated to reach unity at an r value near 2.0 to form a single plasmid complex. Apparently, this is consistent with the increased weight fraction of PEG in the micelle with an increased r value to prevent secondary coalescence.

3.4. Transfection to 293 cells

In vitro transfection to 293 cells was performed in the presence of 100 μM chloroquine using PEG–PLL/pDNA micelles prepared from pDNA and PEG–PLL with varying compositions (12-7, 12-19, 12-48). As shown in Fig. 9, the transfection efficiency was progressively improved by increasing the length of the PLL segment in the PEG–PLL complexing with pDNA. Comparing the micelles with the same PEG–PLL composition but different r value, a higher gene expression was always achieved for the non-stoichiometric micelles ($r > 1.0$) compared to the stoichiometric one. The highest expression was achieved by the 12-48/pDNA micelle with $r = 2.0$. To get insight into the mechanism of this significant effect of the micellar composition on the transfection efficacy, the cellular association of the PIC micelles entrapped with fluorescein-labeled pDNA was estimated by flow cytometry. As shown in Fig. 10(A), there was merely a marginal positive shift in the cytofluorogram for cells applied with 12-7/pDNA and 12-19/pDNA micelles. In contrast, cells applied with 12-48/pDNA micelles revealed a significant increase in the fluorescence intensity regardless of the r value, indicating their efficient association with pDNA. This tendency is clearly represented by a mean value of the fluorescent intensity of 10,000 cells as shown in Fig. 10(B), and is consistent with the transfection results at least when compared to the systems with similar r values. It is noteworthy to discuss this appreciable effect of the PLL length on the cellular association of pDNA-loaded micelles and subsequent transfection results. Apparently, there are no significant differences in the static physicochemical properties, including the size and zeta potential, among the PIC micelles composed of PEG–PLL with varying PLL compositions as seen in Figs. 1, 6 and 8. Nevertheless, as we previously reported [18], the dynamic stability of the PEG–PLL/DNA micelles against the chain exchange reaction with a counter-polyanion, i.e., poly(vinyl-sulfonate) and dextran

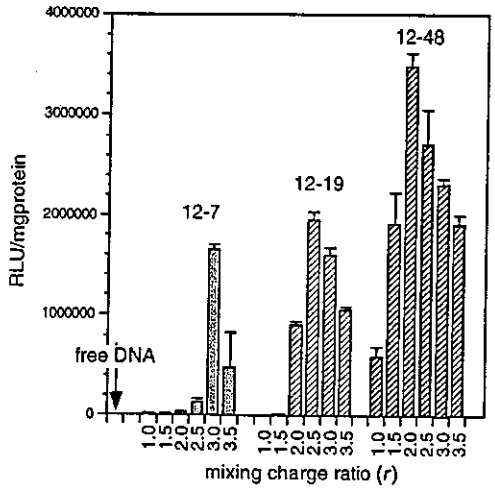

Fig. 9. Transfection efficiency to 293 cells by PIC micelles formed from pDNA and PEG–PLL with varying compositions (12-7, 12-19, and 12-48). 100 μM of chloroquine was included in the transfection medium ($n = 4$, ±S.D.).

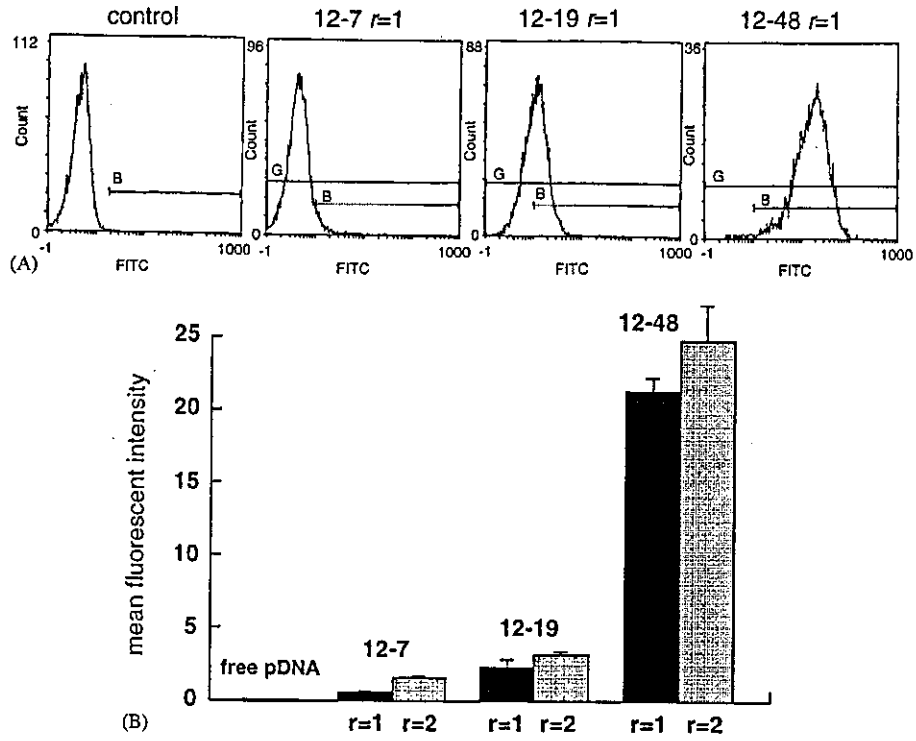

Fig. 10. Cellular association of fluorescein-labeled pDNA entrapped in PIC micelles with varying compositions. (A) Cyto-fluorogram of 293 cells after transfection using PIC micelles. (B) Mean value of the fluorescent intensity for 10,000 cells ($n = 4$, ±S.D.).

sulfate, progressively increased with an increase in the chain length of PLL segment, and further correlates with the nuclease resistance of the micelle-entrapped DNA in the serum-containing medium. Presumably, a substantial degree of DNA dissociation may occur from the micelle composed of 12-7 and 12-19 in the medium or at the cellular surface with an appreciably high local concentration of anionic carbohydrates, thus interfering with the DNA localization into the cellular compartment. This is consistent with our recent results of an animal study demonstrating a higher stability of supercoiled DNA in the blood compartment for the 12-48/pDNA micelles than the 12-19/pDNA micelles [32].

The considerably high cellular association of the 12-48/pDNA system is somewhat surprising, and even controversial to the non-fouling propensity of the hydrated PEG strands through effective steric repulsion. Nevertheless, PEG may have an attractive interaction with each other, or with other components, directly through a hydrophobic interaction or indirectly through the bridge of the bound water molecules, particularly in a concentrated state. Note that PEG can serve as a proton-acceptor to form a hydrogen-bonded complex with a proton-donating polymer such as poly(acrylic acid) [33]. Thus, it may be reasonable to assume a possible interaction between the cellular membrane and the densely localized PEG strands of the micelle shell at the interface.

Although there was observed a clear influence of the r value in the gene expression as shown in Fig. 9, the cellular association of pDNA was less affected by the r value. Typically in the 12-48/pDNA micelles, both the $r = 1.0$ and 2.0 micelles had an appreciably high cellular association of pDNA (Fig. 10B), yet only the $r = 2.0$ micelles achieved a sufficient gene expression. This result suggests a substantial difference in the intracellular fate, including stability, localization, and trafficking, between the micelles with a different r value. It should be noted that a single pDNA complex with a fully condensed structure was formed at $r = 2.0$ (Figs. 3, 4 and 8), yet a correlation of this structural feature to gene expression efficacy is an issue to be clarified in a future study.

When the transfection efficiency of the 12-48/pDNA ($r = 2.0$) micelle is compared to those of other non-viral gene vectors, the micelle showed a comparable gene expression with lipoplex (LipofectAMINE^{TM}), and showed a much higher expression than the PLL/pDNA complexes (PLys-polyplex) as shown in Fig. 11. For non-viral vector systems such as the lipid and polymer-based complexes, an excess cationic charge has been believed to play a substantial role in the enhancement of the gene expression due to an electrostatic interaction with the negatively charged cell surfaces [34–37]. Significant cellular association and appreciable gene expression efficacy of the PIC micelles having a zeta potential with a very small absolute value (~5 mV)